

1 **TITLE: High temporal resolution systems profiling reveals distinct patterns of interferon**
2 **response after Covid-19 mRNA vaccination and SARS-CoV2 infection**

3

4 **AUTHORS**

5 Darawan Rinchai^{1#*}, Sara Deola^{1#}, Gabriele Zoppoli^{2,3§}, Basirudeen Syed Ahamed Kabbeer^{1§},
6 Sara Taleb^{4§}, Igor Pavlovski^{1±}, Selma Maacha^{1±}, Giusy Gentilcore¹, Mohammed Toufiq¹, Lisa
7 Mathew¹, Li Liu¹, Fazulur Rehaman Vempalli¹, Ghada Mubarak¹, Stephan Lorenz¹, Irene
8 Sivieri^{3,5,6}, Gabriella Cirmena², Chiara Dentone², Paola Cuccarolo³, Daniele Roberto
9 Giacobbe^{2,5}, Federico Baldi⁵, Alberto Garbarino³, Benedetta Cigolini³, Paolo Cremonesi⁷,
10 Michele Bedognetti⁸, Alberto Ballestrero^{2,5}, Matteo Bassetti^{2,5}, Boris P. Hejblum⁹, Tracy
11 Augustine¹, Nicholas Van Panhuys¹, Rodolphe Thiebaut⁹, Ricardo Branco¹, Tracey Chew¹⁰,
12 Maryam Shojaei^{11,12}, Kirsty Short^{13,14}, Carl Feng^{15,16}, PREDICT-19 consortium, Susu M.
13 Zughaier¹⁷, Andrea De Maria^{2,5}, Benjamin Tang^{12,18}, Ali Ait Hssain¹⁹, Davide Bedognetti^{1,3&},
14 Jean-Charles Grivel^{1&} and Damien Chaussabel^{1&*}

15

16 1. Research Branch, Sidra Medicine, PO Box 26999, Doha, Qatar

17 2. IRCCS Ospedale Policlinico San Martino, Genoa, Italy

18 3. Department of Internal Medicine and Medical Specialties, University of Genoa, Genoa,
19 Italy

20 4. Division of Genomics and Translational Biomedicine, College of Health and Life Sciences,
21 Hamad Bin Khalifa University, Doha, Qatar

22 5. Division of Infectious Diseases, Department of Health Sciences, University of Genoa,
23 Genoa, Italy

24

- 25 6. Department of Experimental and Clinical Medicine, School of Internal Medicine,
26 University of Florence, Florence, Italy
- 27 7. Emergency Department, E.O. Ospedali Galliera Genova, Italy
- 28 8. Azienda Sanitaria Locale 3 Genovese, Genova, Liguria, Italy
- 29 9. Univ. Bordeaux, Department of Public Health, Inserm U1219 Bordeaux Population Health
30 Research Centre, Inria SISTM, F-33000 Bordeaux, France
- 31 10. Sydney Informatic Hub, The University of Sydney, Sydney, Australia
- 32 11. Nepean Clinical School, University of Sydney, Sydney, New South Wales, Australia;
- 33 12. Westmead Institute for Medical Research, Westmead, New South Wales, Australia.
- 34 13. The University of Queensland, School of Chemistry and Molecular Biosciences, St Lucia,
35 Brisbane, Queensland, Australia;
- 36 14. Australian Infectious Diseases Research Centre, The University of Queensland, Brisbane,
37 Queensland, Australia.
- 38 15. School of Medical Sciences, Faculty of Medicine and Health, The University of Sydney,
39 Sydney, NSW, Australia;
- 40 16. Tuberculosis Research Program, Centenary Institute, The University of Sydney, Sydney,
41 NSW, Australia.
- 42 17. College of Medicine, QU Health, Qatar University, PO Box 2713, Doha, Qatar
- 43 18. Westmead Institute for Medical Research, Westmead, New South Wales, Australia.
- 44 19. Medical Intensive Care Unit, Hamad General Hospital, PO BOX 3050, Doha, Qatar
- 45 #, §, ±, & These authors contributed equally to the work
- 46 * To whom correspondence may be addressed:
- 47 drinchai@sidra.org / drinchai@gmail.com
- 48 dchaussabel@sidra.org / chaussabel@gmail.com

49 **ABSTRACT:**

50 Knowledge of the mechanisms underpinning the development of protective immunity
51 conferred by mRNA vaccines is fragmentary. Here we investigated responses to COVID-19
52 mRNA vaccination via ultra-low-volume sampling and high-temporal-resolution
53 transcriptome profiling (23 subjects across 22 timepoints, and with 117 COVID-19 patients
54 used as comparators). There were marked differences in the timing and amplitude of the
55 responses to the priming and booster doses. Notably, we identified two distinct interferon
56 signatures. The first signature (A28/S1) was robustly induced both post-prime and post-boost
57 and in both cases correlated with the subsequent development of antibody responses. In
58 contrast, the second interferon signature (A28/S2) was robustly induced only post-boost,
59 where it coincided with a transient inflammation peak. In COVID19 patients, a distinct
60 phenotype dominated by A28/S2 was associated with longer duration of intensive care. In
61 summary, high-temporal-resolution transcriptomic permitted the identification of post-
62 vaccination phenotypes that are determinants of the course of COVID-19 disease.

63

64

65

66

67

68

69

70

71

72

73 INTRODUCTION

74 COVID-19 vaccines are critical to the ongoing efforts to control the SARS-CoV-2 coronavirus
75 pandemic. To date, nine vaccines have received some form of approval for use in humans,
76 and phase III trials are ongoing for an additional 11 vaccines (1). Notable differences exist
77 among the vaccine products in terms of their design and the levels of protection they confer,
78 as well as the type, incidence, and severity of adverse events they may elicit. Gaining a
79 comprehensive understanding of the immunological factors underpinning the different
80 responses to various vaccines is a major endeavor. Yet, this knowledge is necessary for guiding
81 timely decisions to modulate vaccination protocols (e.g., the use of different types of vaccines
82 for the priming and booster doses). This information may also assist in matching of individuals
83 with the growing number of available vaccines based on their demographics, health status,
84 or any other relevant clinical/molecular phenotypes.

85 Blood transcriptome profiling measures the abundance of transcripts in whole blood and on
86 a system-wide scale. It was previously employed to comprehensively profile the immune
87 responses elicited by vaccines (2,3). Notably, this approach identified innate immune
88 signatures arising within hours after administering vaccines (4). In a recently published report,
89 Arunachalam et al. described the blood transcriptome profiles measured following the
90 administration of the BNT162b2 mRNA COVID-19 vaccine (5). They reported the presence of
91 an interferon (IFN) signature one day after the priming vaccination that was no longer
92 detectable on day 7. They further found a more comprehensive IFN/inflammatory signature
93 to be present 1 day after administering the booster dose. However, the sampling schedule
94 employed in this study was relatively sparse. And the sample collection time points
95 commonly selected in systems vaccinology studies are based on kinetics established for more
96 conventional vaccines – with sampling at days 1 and 7 often selected since they correspond

97 to the peaks of the innate and adaptive immune responses elicited for instance by the
98 influenza or pneumococcal vaccines (6). However, the precise kinetics of the immune
99 response elicited by mRNA vaccines remains to be established. In the present study we
100 endeavored to profile the blood transcriptome of individuals prior to the administration of
101 the first dose of COVID-19 mRNA vaccine and for the following 9 consecutive days. Subjects
102 also collecting samples for deep serological profiling at three time points. The same sampling
103 and profiling schedule was repeated to assess the response to the second dose of the vaccine.
104 To achieve this, we have adopted a ultra-low volume sampling procedure consisting in the
105 self-collection of few drops of blood (50 ul) by fingerstick (7).

106 Together, this work permitted the precise delineation of a well-orchestrated immune
107 response to COVID-19 mRNA vaccines and identified marked differences in the magnitude,
108 nature, and timing of the transcriptional signatures elicited by prime and boost vaccination.
109 Most notably, differences in temporal patterns of responsiveness revealed distinct
110 components of the interferon response, which is known to play a key role in controlling SARS-
111 CoV-2 infection (8) and was also found here to associate with the subsequent development
112 of the antibody response post-vaccination.

113

114 **RESULTS**

115 **Study design, implementation, and serological profiling**

116 We successfully recruited a cohort of volunteers and implemented a high-frequency sampling
117 protocol. This permitted to ascertain the response to the first and second dose of COVID-19
118 vaccines at 10 consecutive daily timepoints: immediately before vaccination and for 9 days
119 after. We collected samples for serological profiling at three time points: before vaccination
120 and on days 7 and 14 post-vaccination (**Figure 1A**). We implemented a self-sampling blood

121 collection protocol so that subjects could extract small volumes (50 μ l) of RNA-stabilized
122 blood at the required frequency (the approach is described in the Methods section and an
123 earlier publication (7)). RNA sequencing profiles were generated using a cost-effective 3'-
124 biased library preparation protocol (Lexogen QuantSeq), which is optimized for low amount
125 of RNA input. We generated COVID-19-specific antibody profiles from capillary blood samples
126 collected by Volumetric Absorptive Micro Sampling analyzed using a multiplexed Bead array
127 established by our team (see Methods for details). Overall, 23 subjects were enrolled in the
128 study, and the characteristics of this cohort are reported in **Table 1**. They received either two
129 doses of the Pfizer/BioNTech mRNA vaccine (BNT162b2, N = 19) or two doses of the Moderna
130 mRNA vaccine (N = 4). Among those 23 subjects, six had recovered from COVID-19 in the
131 months preceding the administration of the first vaccine dose. In total 440 RNA sequencing
132 profiles were generated, and this extensive dataset was shared publicly in GEO with the
133 accession number GSE190001. The serological profiles included reactivity to a stabilized
134 trimer of Spike protein, the spike protein, its receptor-binding domain, the Nucleo and
135 Envelope proteins, of SARS-CoV2, and the subunit S1 of SARS spike protein. The data are
136 provided in **Supplementary File 1**. The seroreactivity to each of these antigens was dissected
137 by measuring the total IgG, total IgA, and IgM, as well as the finer-scale IgG and IgA subtypes.
138 Serological profiling data showed a rise in the levels of antibodies in the plasma of the subjects
139 post-vaccination (**Figure 1B**), and this included antibodies specific for the SARS-CoV-2 Spike
140 protein, which is targeted by COVID-19 vaccines. No responses to the Envelope protein were
141 detected. Some cross-reactivity was observed with the SARS Spike protein. Notably, higher
142 antibody levels were induced after the first dose in individuals who had been previously
143 infected with the virus (**Figure 1B-C**).

144 Altogether, the implementation of this protocol established the feasibility of obtaining
145 stabilized-RNA blood samples from study-subjects post-vaccination at high-temporal
146 frequencies. We generated a large dataset using a cost-effective RNA-sequencing protocol
147 that served as the basis for subsequent analyses presented in this paper and was deposited
148 in a public repository. A detailed map of the serological profiles of the subjects enrolled in the
149 study was obtained that permitted us to explore the possible associations between blood
150 transcriptional responses and vaccine immunogenicity.

151

152 **The post-prime interferon response peaks at day-2 and correlates with the antibody**
153 **response**

154 Vaccines can elicit innate immune responses that are detectable systemically via blood
155 transcriptome profiling. But not all of them do, which is for instance the case of the aluminum-
156 adjuvanted Hepatitis B vaccine (9). Therefore our first question was whether transcriptional
157 changes could be observed during the first few days following the administration of COVID-
158 19 mRNA vaccines.

159 Analyses were carried out employing a fixed repertoire of 382 transcriptional modules
160 (BloodGen3) that we had recently established and characterized functionally (10)(see
161 methods section for details). Module responses were determined across all time points. The
162 differential gene-set enrichment functions of the dearseq R package were run to assess
163 whether changes observed throughout the nine days post-prime were statistically significant
164 (11). This analysis identified significant temporal changes for 22 of the 382 modules
165 constituting the BlooGen3 repertoire (**Supplementary File 2**).

166 Only seven modules were found to be changed at any given time point during the first
167 three days following the administration of the priming dose of the vaccine (**Figure 2A**). The

168 abundance of four modules was consistently increased across these time points, and all four
169 belonged to the module aggregate A28. Each “module aggregate” regroups sets of modules
170 that showed consistent abundance profiles across a reference set of 16 disease cohorts that
171 were employed for the construction of the BloodGen3 repertoire (see methods and (10) for
172 details). The module aggregate in question (“Aggregate A28”) comprises of six modules. As
173 described in detail in one of our recent publications, all six are associated with interferon
174 responses (10). The gene composition of the modules and the functional annotations are
175 provided herein (relevant information is provided in **Supplementary File 3** and can be
176 accessed interactively via: <https://prezi.com/view/E34MhxE5uKoZLWZ3KXjG/>). The
177 responses observed on days 1 and 2 post-prime were mapped onto fingerprint grid plots,
178 where modules occupy a fixed position and are arranged by aggregate. Each aggregate
179 occupies a given row (**Figure 2A**). Time-course gene-set enrichment analysis confirmed that
180 changes observed over time in four out of six A28 modules were significant. The response
181 profiles of the A28 modules showed a peak on day 2 post-vaccination. This was also visible on
182 a heatmap showing responses at each timepoint across individual subjects (**Figure 2B**). We
183 next examined whether this signature correlated with antibody responses measured 14-days
184 post-prime as well as at 14-days post-boost (**Figure 2C**). For this, correlation analyses were
185 run at the module level within Aggregate A28 using, as the endpoint, fold-changes in antibody
186 levels on days 7 and 14 post-prime and days 7 and 14 post-boost relative to the pre-
187 vaccination baseline (immediately prior to the administration of the first dose of COVID-19
188 mRNA vaccines). “Significance hotspots” were identified when most modules within a given
189 aggregate reached correlation significance thresholds. In the case of the post-prime
190 interferon signature, we identified such significance hotspots on days 2 and 3 post-prime for

191 a subset of three interferon modules, M10.1, M15.127, and M83, while a fourth module,
192 M15.86, also displayed significant correlations across all antibody types, but only on day 2.

193 Thus, we found that an interferon response is induced over the first three days following
194 the administration of the priming dose of mRNA vaccines. Remarkably this signature
195 correlated with the antibody response measured several weeks later, 14 days after the
196 administration of the second dose of vaccine.

197

198 **A decrease in inflammation is accompanied by an increase in adaptive immune response**
199 **genes on day 5 post-prime**

200 We were next interested in characterizing the changes occurring beyond the first three days
201 following administration of the priming dose. In total, 18 modules displayed changes on day
202 4 post-prime, of which 12 showed a decrease in abundance. These modules belonged to three
203 aggregates that have been associated with inflammation (A31, A33, A35). Most changes were
204 observed on day 4, but for some modules, changes were apparent starting on day 3 and
205 continued beyond days 4, day 5, or even 6 (**Supplementary Figure 1**). In our earlier work,
206 modules within the BloodGen3 Aggregate A35 were associated with systemic inflammation
207 mediated by neutrophils and were found to constitute a common denominator across a wide
208 range of pathologies in which systemic inflammation is present (12). The association of A35
209 with inflammatory processes was also ascertained based on the results of the functional
210 profiling analyses and the restriction in transcript expression in the reference datasets (10).
211 Detailed functional annotations can be accessed via interactive circle packing charts:
212 <https://prezi.com/view/7Q20FyW6Hrs5NjMaTUyW/>). Module Aggregate A33 has not been
213 investigated as extensively in any of our prior studies but was clearly associated with
214 inflammation via functional profiling (<https://prezi.com/view/VBqKqHuLWCra3OJOIZRR/>).

215 The peak response post prime was on day 5, with a total of 42 modules showing
216 differences in comparison to the pre-vaccination baseline (**Figure 3**). At this timepoint, most
217 modules showed an increase in abundance (29 were increased and 13 decreased). Some of
218 those modules belonged to aggregates that were associated with adaptive immunity, most
219 notably A27, which is associated with plasmablast responses (three out of five modules were
220 responsive at this timepoint). This association is based on the restriction of the expression of
221 the genes comprising A27 modules in plasma cells observed in a reference dataset including
222 a wide range of cell populations (contributed by Monaco et al. (14)) and by the presence of
223 the plasmablast marker CD38 and other associated genes (*IGJ*, *TNFRSF17*, *TXNDC5*) in one of
224 the A27 modules (M12.15). Detailed annotations and expression profiles of A27 transcripts in
225 the reference datasets can be accessed via <https://prezi.com/view/GgliA0K9kSFHbpVj2I85/>.
226 Other immune-relevant modules found to be increased at this timepoint are associated with
227 T-cells (M12.6 from aggregate A1). Detailed functional annotations for module aggregate A1
228 can be accessed via <https://prezi.com/view/sxap39tKxkmCNTTNIIVO/>). Others were mapped
229 to module aggregates A24 and were associated with oxidative phosphorylation which is
230 known to play a role for instance in T-cell activation (6 out of 11 modules were responsive)
231 (13). Other modules were not yet functionally annotated, including for instance the four
232 responsive modules, out of 15, belonging to aggregate A26. Notably, the signatures observed
233 on day 5 appeared to be transient, and no modules were increased on day 6 post-prime.

234 Taken together, we found the number of responsive modules to peak on day 5 post-
235 prime. A decrease in the abundance of transcripts associated with inflammation was
236 accompanied by an increase in the abundance of transcripts associated with adaptive
237 immune responses. Notably, the latter appeared earlier than seen in response to other
238 vaccines where plasmablast signatures are observed around day 7 post-vaccination (6,14,15).

239 **A post-boost interferon signature peaks on day 1 and correlates with antibody responses**

240 After delineating temporal responses post-prime, we examined changes after the
241 second dose of COVID-19 mRNA vaccines. Time-course gene set enrichment analysis
242 identified significant temporal changes for 311 of 382 modules comprising the BloodGen3
243 repertoire (**Supplementary File 4**). After the booster dose, the peak number of responsive
244 modules occurred on day 1, with 261 responsive modules or about two-thirds of the 382
245 modules constituting the BloodGen3 repertoire (**Figure 4**). This number decreased sharply
246 afterward, with 115 responsive modules on day 2 and only 9 responsive modules on day 3.
247 The kinetic and amplitude of the post-boost response contrasted markedly with that
248 observed post-prime, when, as described above, the number of responsive modules after the
249 first dose instead peaked on day 5, with changes found in 42 modules at that timepoint.

250 As seen from the fingerprint grid plot, the day 1 post-boost response was extensive
251 and polyfunctional (**Figure 4**). An overall decrease in abundance was observed for aggregates
252 broadly associated with lymphocytic cells (Aggregates A1-A8) and increased for module
253 aggregates associated with myeloid cells, inflammation, and circulating erythroid cells
254 (Aggregates A33-A38). In addition, a marked increase in the abundance of modules associated
255 with interferon responses was also observed (Aggregate A28). We compared the day 1
256 response fingerprint of the COVID-19 mRNA booster vaccine to fingerprints derived from
257 patients with a wide range of pathologies. These included sixteen reference datasets
258 encompassing infectious and autoimmune diseases, as well as cancer, solid organ transplant
259 recipients, among others (these cohorts are described in our previously published work
260 (10,16); the respective blood transcriptome fingerprint collections are accessible via a
261 dedicated web application: <https://drinchai.shinyapps.io/BloodGen3Module/>). In addition,
262 we analyzed two original COVID-19 blood transcriptome datasets: one cohort comprising 77

263 Covid-19 patients with disease severities ranging from mild and moderate to severe (the
264 “PREDICT-19 consortium Italian cohort dataset” – see methods and published study protocol
265 for details (17)), while the second cohort comprised 40 COVID-19 patients recruited at the
266 time of admission to the intensive care unit (ICU) (“IMPROVISE cohort whole blood dataset”).
267 These high-level comparisons showed, firstly, that the extent of the changes associated with
268 the day 1 response to the second dose of the COVID-19 mRNA vaccine was consistent with
269 that observed in some patient cohorts with acute infections (**Figure 4**). More specifically, they
270 were found to most resemble the responses seen in a cohort of subjects with influenza
271 infection, with a marked interferon response (A28) and an inflammation signature (A33, A35).
272 At a higher level, these response patterns were also generally consistent with those observed
273 in patients with a COVID-19 infection. However, the changes that occurred in response to the
274 vaccinations were not as extreme as those found, for instance, in patients with sepsis or with
275 the most severe form of COVID-19 (i.e., the IMPROVISE dataset) (most notably for
276 inflammation [A33, A35] and erythroid cell responses [A36-A38]).

277 Overall, the BloodGen3 transcriptome fingerprint observed on day 1 after the second
278 vaccine dose contrasted markedly with the fingerprint observed on day 1 post-prime. Yet, the
279 interferon response signature was found to be a common denominator between the
280 responses to the first and second doses, as it was observed in both cases in the first few days
281 following administration of the vaccine. We therefore began to dissect the post-boost
282 response by examining this interferon response signature in more detail.

283 Following the administration of the booster dose, the interferon response was
284 noticeably sharper in comparison to the post-prime response and peaked on day 1 instead of
285 day 2 (**Figure 5A**). This was illustrated by the difference in the maximum average module

286 response, which was close to 50% of the constitutive transcripts on day 2 post-prime and
287 greater than 80% on day 1 post-boost.

288 We decided to then perform hierarchical clustering to identify subsets of modules within
289 the A28 aggregates that might group together based on patterns of transcript abundance
290 across all subjects and timepoints. Two sets of three modules each were, thus, identified
291 within the A28 aggregate. The first set comprised modules M8.3, M10.1, and M15.127
292 (referred to as A28/S1), and the second set comprised modules M16.64, M13.17, and M15.86
293 (referred to as A28/S2). Interestingly, we observed post-prime that, while modules in A28/S1
294 peaked on day 2, those belonging to A28/S2 peaked on day 1 (**Figure 5B**). Furthermore,
295 A28/S1 modules showed an extended peak post-boost, with day 2 levels being almost
296 identical to those of the day 1 peak, while A28/S2 modules peaked sharply on day 1, with
297 levels decreasing rapidly thereafter. These findings suggest that both sets of modules
298 measured distinct types of interferon response. Indeed, public datasets in which responses
299 to type 1 interferon were measured *in-vivo* indicated that A28/S1 modules are likely to
300 represent type 1 interferon responses (**Figure 5B**), while we postulated that A28/S2 modules
301 might represent a type 2 interferon response. Modules forming the A28/S1 set comprise
302 some of the better recognized “canonical” interferon response genes, such as Oligoadenylate
303 Synthetase family members (OAS1, OAS2, OAS3, OASL), Interferon Induced Protein family
304 members (IFI6, IFI27, IFI35, IFI44, IFI44L), as well as Interferon Induced Protein With
305 Tetratricopeptide Repeats family members (IFIT1, IFIT3, IFIT5) (10). Modules forming the
306 A28/S2 set comprise instead most notably members of the Nuclear Antigen family members
307 SP100, SP110 and SP140, which are associated with interferon gamma signaling, as well as
308 transcription factors IRF9 and STAT2. Composition and functional annotations for A28
309 modules can be explored further at: <https://prezi.com/view/E34MhxE5uKoZLWZ3KXjG/>.

310 Finally, a strong association was found between the post-boost interferon signature and
311 the subsequent development of an antibody response. Indeed, positive correlations were
312 observed for all six A28 modules that reached significance on days 1, 2, and 3 post-boost.
313 Notably, this differed from the post-prime interferon response, for which significance was
314 reached only for four of the six modules and only on days 2 and 3.

315 Taken together, the high temporal resolution profiling results permitted the delineation
316 of distinct patterns of post-prime and post-boost interferon responses. The timing of the
317 responses observed at the individual module level contributed to the definition of the two
318 distinct sets of interferon modules. One set was associated with responses to type I interferon
319 *in-vivo* and dominated the post-prime response, with a peak on day 2. The post-boost
320 response showed a strong induction of both sets and also peaked on day 1.

321

322 **Inflammation and erythroid cell signatures peak sharply on day 1 post-boost**

323 We continued the dissection of the day 1 post-boost signature, focusing this time on
324 responses associated with inflammation and circulating erythroid cell precursors.

325 Aggregates A33 and A35, which are associated with inflammation, tended to decrease
326 from day 4 through day 6 post-prime but displayed instead a sharp and transient increase in
327 abundance post-boost. Indeed, a well-delineated response peak was observed on day 1 post-
328 boost for both the A33 and A35 modules (**Figure 6**), but in contrast to the interferon response
329 (A28/S1), it did not extend beyond the first day. Three distinct response patterns were
330 identified via hierarchical clustering among the 21 modules that formed aggregate A35. The
331 “A35/S1” set comprised five modules, while “A35/S2” and “A35/S3” comprised ten and six
332 modules, respectively. The distinction between those three A35/inflammation module sets
333 was rather more subtle than was the case for the A28/interferon sets. Indeed, all three

334 module sets peaked on day 1 post-boost. Differences were rather apparent in the inflection
335 of changes measured on days 2 and 3 post-boost and in the “recovery phase”, as abundances
336 appeared to dip below the baseline and progressively rise to reach pre-vaccination levels. The
337 underlying biological factors driving the grouping of the modules to those three distinct sets
338 could not be identified at this time.

339 Modules for three aggregates broadly associated with erythroid cell signatures also
340 displayed a sharp but transient increase in transcript abundance on day 1 post-boost.
341 However, the abundance tended to dip afterward, with a low peak on day 4 post-boost,
342 before recovering by day 7. Functionally, this signature was found to be most prominently
343 associated with immunosuppressive states, such as late-stage cancer or pharmacological
344 immunosuppression (16), which is consistent with published functional studies (18,19). We
345 also found such signatures were associated with more severe manifestations in babies
346 infected with Respiratory Syncytial Virus (RSV) (16). Moreover, erythroid precursors have
347 been recently associated with COVID most severe clinical outcomes (20). Finally, we did not
348 find evidence of an association between the day 1 post-boost inflammation or erythroid cell
349 signatures and the antibody responses.

350

351 **A plasmablast signature peaks on day 4 post-administration of the booster dose and**
352 **correlates with antibody responses**

353 After the booster dose, the number of responsive modules peaked sharply on day 1,
354 then rapidly subsided beyond day 2, with the number of responsive modules on days 3, 4, 5,
355 and 6 being reduced to 8, 11, 3, and 2, respectively. Yet, changes within this later timeframe
356 are meaningful, as they specifically concern the set of five modules comprising aggregate A27,
357 which is associated with the presence of antibody-producing cells in the peripheral blood.

358 Three of the five A27 modules showed significant alterations after the booster dose (M16.60,
359 M13.32, M12.15) (**Figure 6**). The proportion of differentially expressed transcripts in each
360 module was relatively modest (with an average of 15% at the peak of response), especially in
361 comparison with the interferon signatures described above (with an average of >80% for
362 some modules at the response peak). Yet, the trajectories of the five A27 modules were
363 relatively consistent, with only one of the modules (M15.110) showing a different pattern,
364 i.e., a peak on day 6, slightly above the levels observed on day 4. We also examined the
365 association of this post-boost plasmablast signature with the antibody response and found a
366 significant association starting from about day 3 and lasting until day 7 post-boost (**Figure 6**).

367 In summary, COVID-19 mRNA vaccination induced a plasmablast response that peaked on
368 day 4 post-vaccination. This was unexpected since such signatures typically are measured
369 around day 7 post-vaccine administration (e.g., in the case of influenza or pneumococcal
370 vaccines (6)). We were also able to demonstrate a logical association between this post-boost
371 plasmablast signature and the subsequent development of humoral immunity.

372

373 **Patterns of interferon induction elicited by COVID-19 mRNA vaccines are also observed** 374 **among COVID-19 patients**

375 Our work identified the interferon response as the most upstream factor associated with the
376 development of humoral immunity following COVID-19 mRNA vaccination. High-temporal
377 resolution profiling identified distinct patterns of interferon induction post-prime and post-
378 boost and we next decided to determine whether similar response patterns could be
379 identified among patients with COVID-19 disease.

380 We relied for this on the original blood transcriptome data from the PREDICT-19
381 consortium Italian COVID-19 cohort comprising 77 patients with a wide spectrum of disease

382 severity. We used the response values for the six interferon modules from Aggregate A28 to
383 map individual COVID-19 patient samples along with post-vaccine samples on the same t-SNE
384 plot (**Figure 7A**). First, we confirmed that there was no apparent separation of the vaccination
385 and COVID-19 patient cohorts, and that batch correction was therefore not warranted before
386 proceeding with comparative analyses (**Supplementary Figure 2**). This is consistent with the
387 results of meta-analyses we have previously conducted at the module level (16). To help with
388 the interpretation, k-means clustering was performed using the consolidated set of samples,
389 resulting in the formation of eight distinct clusters. Next, we examined the distribution of
390 samples from the vaccine and COVID-19 cohorts across the tSNE plot and among the eight
391 clusters. Timepoints at which an interferon response was detectable in vaccinated subjects
392 were of particular interest. Indeed, day 1 and day 2 post-prime samples (P1, P2), while
393 preferentially found in Clusters 1 and 5, appeared to be distributed across the entire t-SNE
394 plot. This is in contrast with day 1 and day 2 post-boost vaccination samples (B1, B2), which
395 were almost exclusively found in Cluster 5. A set of COVID-19 patients also co-localized in
396 Cluster 5, while others were found scattered across clusters, especially Clusters 1, 2, 6, and 3.
397 Interferon responses were detectable in all these clusters, but with important nuances. For
398 one, samples from Cluster 5 showed by far the most potent responses, with responses seen
399 in most cases across all six interferon modules, which was consistent with the post-boost
400 vaccine response (**Figure 7B**). In comparison, the response was less pronounced in samples
401 from Cluster 1, which was dominated by modules associated with type I interferon responses
402 (the A28/S1 set comprising M10.1, M8.3 and M15.127 described above). This pattern of
403 response was more consistent with the post-prime vaccine response. Signatures for samples
404 forming Clusters 2 and 6 were not well-defined and were in some cases absent, yet these
405 clusters also included COVID-19 patients. Samples forming Cluster 3 displayed a peculiar

406 signature, with an increase in the abundance of modules belonging to the A28/S2 set
407 (M15.64, M13.17, and M15.86) concomitantly with a decrease in modules forming A28/S1.
408 Among the samples forming this cluster, this pattern was most apparent for the COVID-19
409 patients.

410 Thus, we employed here the interferon responses observed post COVID-19
411 vaccination as a benchmark for the interpretation of COVID-19 patient signature. We were
412 able to establish that most COVID-19 patients display responses consistent with those found
413 post-vaccination, which, as established in this study, were associated with the development
414 of potent humoral responses. However, a subset of patients displayed patterns of interferon
415 response that are not typically seen in vaccinated individuals. It can thus be surmised that the
416 later patterns of interferon response might either be suboptimal or possibly even pathogenic.
417

418 **The atypical interferon response signature observed in COVID-19 patients is associated**
419 **with a worse course of disease**

420 The fact that some COVID-19 patients failed to display robust “post-vaccine-like” interferon
421 responses may be due to either a defective innate immune response, which may lead to
422 more severe disease course, or conversely to activation thresholds not being reached in
423 patients presented with milder disease.

424 Thus, we next examined patterns of interferon response in another original COVID-19
425 disease cohort, comprised exclusively of patients enrolled at the time of admission in the ICU
426 (the IMPROVISE cohort, which was also described above). As described above, we again
427 mapped individual COVID-19 patient samples along with post-vaccine samples on a t-SNE plot
428 based on similarities in the patterns of interferon responsiveness across the six A28 interferon
429 modules (**Figure 8A**). COVID-19 subjects were found to again be distributed throughout

430 multiple clusters. Patients who co-localized with day 1 post-boost vaccine samples tended to
431 have relatively short ICU stays (in Cluster 5 with potent A28/S1 and A28/S2 responses), and
432 only a few patients co-localized with day 2 post-prime samples in Cluster 3, which was
433 characterized by a more prominent A28/S1 signature compared with A28/S2. Furthermore,
434 distinct groups of patients in Clusters 1 and 6 displayed the peculiar pattern of interferon
435 response dominated by A28/S2 that was identified earlier among patients enrolled in the
436 PREDICT-19 cohort. Notably, patients from the IMPROVISE cohort displaying this pattern of
437 interferon response showed significantly lengthier stays in the ICU compared to patients
438 displaying patterns of interferon response that are consistent with those observed post-
439 vaccination (**Figure 8B** comparing left and right cluster: for length of hospital stay, t-test, $p =$
440 $0.006 (**)$, mechanical ventilation days $p = 0.016 (*)$ and ICU stay $p = 0.012(*)$).

441 Thus, in a cohort of subjects uniformly presenting with severe disease, post-prime-like
442 patterns of interferon response dominated by A28/S1 were less prevalent. Post-boost-like
443 pattern of interferon response characterized by robust A28/S1 and A28/S2 signatures were
444 observed instead in most patients. A notable exception were patients presenting with
445 patterns of response dominated by A28/S2, not observed previously following vaccination
446 but which were found again in this second independent COVID-19 dataset. In this context we
447 could also establish that such response is associated with a worse disease course. This overall
448 supports the notion that patients harboring this signature may fail to mount an effective
449 immune response against SARS-CoV-2.

450

451

452

453 **The peculiar interferon response phenotype observed in COVID-19 patients is not typically**
454 **found in the context of other infections**

455 Finally, we asked whether the A28/S2-dominated interferon response pattern associated with
456 worse disease outcomes in COVID-19 patients was also commonly found in other infectious
457 disease.

458 For this we first developed a standard definition of “Interferon Response
459 Transcriptional Phenotypes” (IRTPs): the two distinct signatures described above, A28/S1 and
460 A28/S2, were employed as “traits” for the definition of three main phenotypes observed
461 following vaccination and in response to SARS-CoV2 infection. 1) IRTP I encompassed A28/S1-
462 dominated patterns of response: "A28/S1⁺⁺A28/S2⁺⁺", "A28/S1⁺⁺A28/S2⁰" and
463 "A28/S1⁺A28/S2⁺⁺" (see the method section for details). 2) IRTP II corresponded to a pattern of
464 interferon response characterized by the strong induction of both components:
465 A28/S1⁺⁺A28/S2⁺⁺. 3) IRTP III encompassed the A28/S2-dominated patterns of interferon
466 response: "A28/S1⁻A28/S2⁺⁺⁺", "A28/S1⁻A28/S2⁺⁺", "A28/S1⁰A28/S2⁺⁺⁺", "A28/S1⁰A28/S2⁺⁺" and
467 "A28/S1⁻A28/S2⁰". These three IRTPs were in turn employed for the stratification of our
468 vaccination cohort at early time points following administration of the priming and booster
469 doses, as well as both of our COVID-19 cohorts and of several reference cohorts of patients
470 which we had generated as part of one of our earlier studies (10), focusing more particularly
471 on pathologies known to elicit robust interferon responses, including viral infections
472 (influenza, RSV, Human Immunodeficiency Virus [HIV]), tuberculosis or systemic lupus
473 erythematosus (SLE) (**Figure 8C**).

474 Interferon Response Transcriptional Phenotype I (IRTP I), that we posit corresponds
475 to a response dominated by type 1 interferon (IFN α , IFN β), in absence of a substantial type 2
476 interferon (IFN γ), was found in $\pm 1/3$ of the vaccinated subjects at peak response on day 2

477 post-prime (**Figure 8C**: P2). It was however absent at peak response post-boost (B1). Similarly,
478 IRTP I was found among COVID-19 patients belonging to the PREDICT-19 cohort (although in
479 only about 10% of patients), but not among those belonging to the IMPROVISE cohort, who
480 presented with more severe disease. IRTP I was otherwise also found in $\pm 10\%$ of subjects
481 across most of our reference cohorts. However, as was the case of our severe COVID-19
482 cohort, it was absent in the comparator cohort comprised of patients with bacterial sepsis. In
483 the context of mRNA vaccination, IRTP II, which is characterized by the robust induction of
484 both A28/S1 and A28/S2 components, was observed following the booster dose in 95% of
485 samples profiled on day 1, which corresponds to the peak response. The priming dose of
486 Covid-19 mRNA vaccines was able to induce both components robustly but in only 48% of
487 samples at peak (day 2 post-prime). IRTP II was otherwise also prevalent in COVID-19 patients,
488 which is consistent with our earlier observation. It was also found in most samples in the other
489 pathologies employed as comparators – except for RSV and bacterial sepsis (40% and 48%,
490 respectively). Interferon response transcriptional phenotype III (IRTP III), which is
491 characterized by an A28/S2-dominated response was observed only rarely post-COVID-19
492 mRNA vaccination. It was however prevalent among COVID-19 patients, with 25% and 22% of
493 subjects with this phenotype in the PREDICT-19 and IMPROVISE cohorts, respectively.
494 However, it was not observed in patient with tuberculosis, influenza virus or HIV infection.
495 IRTP III is on the other hand found in 13% of patients with RSV infection and reached its peak
496 prevalence in patients with bacterial sepsis (36%).

497 In summary, those results show that in most instances both components of the
498 transcriptional interferon response can be robustly induced following COVID-19 vaccination
499 or viral infection (i.e. corresponding to IRTP II). However, incomplete patterns of induction
500 can also be observed in some circumstances. We hypothesize that this may be due: 1) to

501 activation thresholds not being reached, in the case of IRTP I or 2) to subjects failing to mount
502 an effective interferon response, in the case of IRTP III, which in the context of SARS-CoV-2
503 infection appears to impact their ability to control the infection. Notably, besides COVID-19,
504 IRTP III phenotypes were only observed in a limited set of pathologies, including infection
505 caused by RSV, a virus that is known to interfere with the interferon response (21,22), and
506 bacterial sepsis that is characterized by a dysregulated host response to infection (23).

507

508 **DISCUSSION**

509 Relatively little is known about the types of *in-vivo* immune responses elicited by mRNA
510 vaccines in humans. To address this, we employed bulk blood transcriptomics to map the
511 immune changes taking place *in-vivo* after the administration of priming and booster doses
512 of COVID-19 vaccines in adult volunteers. We did so at a high-temporal resolution, collecting
513 small amounts of blood before and for nine consecutive days after the administration of the
514 priming and booster doses of COVID-19 mRNA vaccines. The use of blood transcriptomics
515 eliminated the need to choose a panel of analytes to measure vaccine responses, which is
516 one source of bias. The daily collection and profiling schemes adopted eliminated the need
517 to choose specific timepoints for measuring the response, thus eliminating a second source
518 of bias.

519 Profiling blood transcript abundance post-prime and -booster doses of COVID-19
520 mRNA vaccines at a high-temporal resolution revealed a well-orchestrated sequence of
521 immune events (**Figure 9**). The immune signatures elicited following the administration of the
522 two doses of mRNA vaccines differed drastically. Relatively modest changes were observed
523 post-prime that manifested primarily as the induction of interferon-response signatures that
524 were detectable over the first three days following the injection of the first dose. This was

525 followed by a more subtle response that could be attributed to the priming of the adaptive
526 response between days 4 and 6. Indeed, a decrease in the abundance of transcripts for
527 modules associated with inflammation was observed over these three days, which included
528 an increase in transcripts associated with plasma cells and T-cells on day 5. No further changes
529 were detected beyond day 6. After the booster dose, the plasmablast response was more
530 robust and peaked on day 4, but was not accompanied by a T-cell response peak as was the
531 case post-prime. Notably, in studies assessing blood transcriptional responses to vaccines, the
532 peak plasmablast response is typically observed on day 7, as it is, for instance, with influenza
533 and pneumococcal vaccines (6,14,15). As a result, sampling schedules in common use are
534 designed to capture changes on days 1, 7, and sometimes day 3, but would miss the peak of
535 the adaptive response to COVID-19 mRNA vaccines observed in our study. In addition to
536 eliminating potential blind spots, high-frequency sampling and profiling also permit the
537 precise resolution of signatures that show the complex kinetics of a response; for instance,
538 the erythroid cell signature peaks sharply post-boost and recedes well below baseline over
539 several days before recovering. The trajectory of this signature may be of significance in the
540 context of vaccination, as we recently described its association with immunosuppressive
541 states, such as late-stage cancer and maintenance therapy in liver transplant recipients (16).
542 In the same work, we found this signature to be strongly associated with the development of
543 a more severe disease in subjects with acute respiratory syncytial virus infection; and we
544 furthermore putatively associated this signature with populations of circulating erythroid
545 cells found to possess immunosuppressive properties (18).

546 Arunachalam et al. previously described the elicitation of qualitatively distinct innate
547 signatures on day 1 following the administration of priming and booster doses of COVID-19
548 mRNA vaccines, with the former inducing an interferon response and the latter a mixed

549 response that also presented an inflammatory component (5). Our findings are consistent
550 with these earlier observations and, employing a high-frequency sampling and profiling
551 protocol, permitted to further dissect those responses. Most notably, while interferon
552 responses appear *a priori* as the common denominator between the post-prime and post-
553 boost responses, the temporal pattern of response that we observed indicates that these are,
554 in fact, qualitatively and quantitatively distinct. This was best evidenced by the differences in
555 the timing of the response peak, which corresponded to day 2 post-prime and day 1 post-
556 boost. The kinetics of the response post-boost is, therefore, most consistent with what is
557 observed following injection of a single dose of influenza vaccine (6). Interestingly, a further
558 investigation of the patterns of response among the six modular components of the
559 interferon responses (module Aggregate A28) identified two distinct sets of modules. These
560 two sets of three modules each, A28/S1, and A28/S2, displayed distinct kinetics and
561 amplitude of response post-prime and post-boost. We have described, in an earlier report,
562 that distinct interferon modules could be employed to stratify patients with systemic lupus
563 erythematosus (24). Here we sought to specifically determine whether “post-prime-like”
564 patterns (i.e., dominated by A28/S1 – IRTP I) or “post-boost-like” patterns (i.e., with potent
565 induction of both components: A28/S1++, A28/S2++ - IRTP II) could be identified among
566 COVID-19 patients. Indeed, since those were associated with the subsequent development of
567 humoral immunity in the context of vaccination it may be surmised that it would also be the
568 case during the course of SARS-CoV-2 infection. This question was made particularly relevant
569 in the context of COVID-19 disease, since it has been reported that failure to induce interferon
570 responses is associated with worse disease outcomes (8,25–27). In the PREDICT-19 cohort,
571 composed by patients with predominantly mild or moderate pathology, both phenotypes
572 were indeed observed, along with a third “atypical” phenotype that was not observed post-

573 vaccination. This latter phenotype is dominated instead by A28/S2, with A28/S1 abundance
574 low or even decreased (IRTP III). Notably, in a cohort of severe patients, both A28/S1++
575 A28/S2++ (“post-boost-like” / IRTP II) and A28/S2>S1 (“atypical” / IRTP III) phenotypes were
576 also observed, with the latter being associated with extended lengths of stay in the ICU.
577 However, IRTP III did not appear to be preferentially associated with death in this setting,
578 which may be due to the supportive care provided to the patients. While, overall, our
579 observations support the notion that failure to mount robust interferon responses is
580 associated with a less favorable course of the disease, they also show that the response
581 elicited in these patients may be of a peculiar type, but is altogether not entirely defective
582 (i.e., with only one component. A28/S1, being primarily affected). One possibility is that this
583 peculiar response pattern may be associated with the presence of endogenously produced
584 autoantibodies that neutralize interferon, as has been previously described (27,28). The high
585 incidence of the IRTP III phenotype observed in patients with bacterial sepsis (about 1 in 3),
586 however suggests that other mechanisms may be at play. Taken together, it is not possible
587 for us to be conclusive on this point at this time and further investigations are thus warranted.

588 Other points remain to be elucidated. This includes the timing of the adaptive response
589 to mRNA vaccines, which appears to rise and peak several days earlier than what is normally
590 observed in responses to other vaccines (\pm 7 day peak). The priming mechanism underpinning
591 the robust polyfunctional response observed on day 1 post-boost remains to be determined
592 as well. And in particular, whether or not such a response, which would typically be
593 considered to be innate, is in fact antigen-specific. Interestingly, in that respect, the subjects
594 who were previously infected but recovered from COVID-19 did not display a noticeable day
595 1 inflammatory response, and their immune systems behaved like those of naïve individuals.
596 However, the number of recovered subjects was small, and the study was not designed to

597 directly address this question. Hence, further investigations will also be necessary. Notably,
598 the greater amplitude of responses observed post-boost and the presence of an inflammatory
599 component is also consistent with previous reports of the increase in the incidence of side
600 effects/discomfort following COVID-19 mRNA vaccine booster doses (29,30).

601 Thus, while this study contributes to a better understanding of drivers of mRNA vaccines
602 immunogenicity it can also serve as a resource to help inform the design of studies
603 investigating vaccine responses. Indeed, a decrease in sequencing costs provides laboratories
604 an opportunity to employ transcriptome profiling approaches in novel ways. One of them
605 being the implementation of high-temporal resolution profiling protocols. An advantage of
606 the delineation of transcriptome responses at high-temporal resolution is that it is doubly
607 unbiased, i.e., there is no need to select transcripts for inclusion in a panel because RNA
608 sequencing measures all transcript species present in a sample. Similarly, there is no need to
609 select specific timepoints for assessing the vaccine response, as all timepoints were profiled
610 within a given time frame. An obvious advantage of the approach is that it permits the
611 removal of potential blind spots and the detection of changes that may otherwise be missed
612 by more sparse sampling protocols. In addition to eliminating potential blind spots high-
613 frequency profiling data helped resolve the vaccine response more precisely. This was the
614 case in our study of the interferon response, with the delineation of two distinct components
615 having been much more difficult if not for the resolution of peaks of response over the first
616 three days post first and second doses of vaccines. Some of the practical elements that may
617 contribute to making the routine implementation of the high-temporal resolution
618 transcriptomics approach viable include, as mentioned earlier, a substantial decrease in the
619 cost of RNA sequencing, especially 3'-biased methodologies. Along the same lines recent
620 publications showed, through down-sampling analysis, that much fewer deep reads than

621 usual are adequate for biomarker discovery projects, which could lead to further reductions
622 in the cost of RNA sequencing assays (31), with the lower costs permitting larger sample sizes
623 or, as in this case, a higher sampling frequency. Another consideration is the availability of
624 solutions for the in-home self-collection of samples. This is the case for the collection of RNA-
625 stabilized blood with our custom method, which could be further improved. Novel solutions
626 are also being put forward that could permit the implementation of these methods at scale
627 (32). Finally, as we have shown, it is possible to implement the self-collection of samples for
628 serology profiling within a vaccinology study.

629 There were several limitations to our study. While the sample size was adequate for an
630 initial discovery phase, a larger study cohort would help to better resolve inter-individual
631 variations. The dataset we generated, however, has been made available for reuse, and it
632 should be possible to integrate and consolidate this dataset with those generated in follow-
633 on studies by us and others (16). Follow-on studies would need to be purposely designed to
634 formally address specific questions, for instance, comparing responses in individuals who had
635 previously been exposed to SARS-CoV-2 with those in naïve individuals. It would also be
636 interesting to compare responses elicited by the Pfizer/BioNTech and Moderna vaccines,
637 which was not possible in our study due to the small numbers of individuals that received the
638 Moderna vaccine. Indeed, although we hoped it would be possible to obtain more balanced
639 sample sizes for a more detailed comparison, the speed at which the vaccinations were rolled
640 out among our target population of healthcare workers meant we had very little control over
641 the number of volunteers that received the different types of vaccines or their status as naïve
642 or previously exposed individuals. It would also have been particularly interesting to enroll
643 patients from different age categories, especially the elderly population, but this again proved
644 impossible.

645 In conclusion, a several COVID-19 vaccines have already been approved for use in humans,
646 and an even greater number of them are currently in phase III trials (>20) (33). The data
647 presented herein suggest that high-temporal-resolution blood transcriptomics would provide
648 a valuable means to precisely map and compare the types of responses elicited by the
649 different types of COVID-19 vaccines. Similarly, this approach could potentially be
650 implemented to characterize and compare vaccine response profiles in populations that do
651 not respond optimally to vaccines (e.g., in the elderly, immunosuppressed, and during
652 pregnancy). This study also contributed to a better understanding of drivers of mRNA vaccines
653 immunogenicity and identified interferon signatures as early indicators of the potency of the
654 humoral immune response elicited in individual subjects. It also led to the definition of
655 functional interferon response phenotypes among COVID-19 patients which were associated
656 with different disease trajectories. In particular, mechanisms underlying the development of
657 dysfunctional interferon responses remain to be elucidated, which may yield important
658 insights into pathogenesis of severe COVID-19 disease.

659

660 **METHODS**

661 **Subject recruitment:**

662 COVAX Cohort: We enrolled adult subjects eligible to receive a COVID-19 vaccine who were
663 willing to adhere to the sampling schedule. The protocol was approved by Sidra Hospital IRB
664 (IRB number 1670047-6), and all participants gave written informed consent. Inclusion criteria
665 matched the clinical eligibility for receiving the vaccine, and the only exclusion criterium was
666 to have received a first dose of any COVID-19 vaccine. Twenty-three subjects were enrolled,
667 and the median age was 38 years (29-57); 20 of the subjects received the Pfizer vaccine and
668 three the Moderna vaccine. The demographics, health status at accrual, and vaccination side

669 effects are shown in Table 1. Vaccination and booster intervals were typically 21 days for
670 Pfizer and 29 days for Moderna.

671

672 IMPROVISE cohort: Adult subjects with severe COVID-19 were enrolled in this cohort under
673 the Hamad Medical Corporation IRB approval (MRC-05-007). Blood samples were collected
674 at multiple timepoints during patients' ICU stay (timepoint 1 was taken at ICU admission;
675 timepoints 1 to 4 were seven days apart). Subjects with burn and trauma, immunological
676 diseases, receiving immunosuppressive treatment, with other immune-related conditions, or
677 with a previous COVID-19 infection were excluded. For this analysis, 40 severe COVID-19
678 patients were included, with a median age of 52 (range = 30 to 92). The clinical parameters
679 of those patients included gender, ICU and hospital stay, mechanical ventilation duration,
680 ECMO initiation, comorbidities, outcomes (death/recovery), nosocomial infection onset, and
681 plasma therapy. Samples were also collected from control subjects who were adults and did
682 not: 1) present with an infectious syndrome during the last 90 days, 2) experience extreme
683 physical stress within the last week, 3) received during the last 90 days a treatment based on:
684 antivirals; antibiotics; antiparasitic; antifungals; 4) received within the last 15 days, a
685 treatment based on non-steroidal anti-inflammatory drugs; 5) received during the last 24
686 months a treatment based on: immunosuppressive therapy; corticosteroids; therapeutic
687 antibodies; chemotherapy and 6) a person with a history of: innate or acquired immune
688 deficiency; hematological disease; solid tumor; severe chronic disease; surgery or
689 hospitalization within the last 2 years; pregnancy within the last year; participation to a phase
690 I clinical assay during the last year; participation to a phase I clinical assay during the last year;
691 pregnant or breastfeeding women; a person with restricted liberty or under legal protection.

692

693 PREDICT-19 Cohort:

694 The “Predicting disease progression in severe viral respiratory infections and COVID-19”
695 (PREDICT-19) Consortium is an international consortium formed by a group of researchers
696 who share common interests in identifying, developing and validating clinical and/or
697 bioinformatics tools to improve patient triage in a pandemic such as COVID-19 (17). The
698 PREDICT-19 Italian cohort comprises adult subjects with mild, moderate, or severe COVID-19
699 diagnosed by real-time PCR on nasopharyngeal swab who were consented and enrolled at
700 E.O. Ospedali Galliera, and IRCCS Ospedale Policlinico San Martino, Genoa, Italy (Ethics
701 Committee of the Liguria Region (N.CER Liguria 163/2020- ID 10475). Blood samples were
702 collected during hospitalization. Subjects with burn and trauma, immunological diseases,
703 receiving immunosuppressive treatment for underlying disorders before COVID-19 diagnosis,
704 with other immune-related conditions, or with a previous COVID-19 infection were excluded.
705 For this analysis, ten healthy subjects and 103 COVID-19 patients were included, with a
706 median age of 61.76 (range = 26 to 86).

707

708 **Sampling protocol:**

709 COVAX Cohort: For transcriptomics applications for the COVAX study, after puncturing the
710 skin with a finger stick, 50 µl of blood was collected in a capillary/microfuge tube assembly
711 supplied by KABE Labortechnik (Numbrecht, Germany) containing 100 µl of tempus RNA-
712 stabilizing solution aliquoted from a regular-sized tempus tube (designed for the collection of
713 3 ml of blood and containing 6 ml of solution; ThermoFisher, Waltham, MA, USA). This
714 method is described in detail in an earlier report (7), and the collection procedure is illustrated
715 in an uploaded video: <https://www.youtube.com/watch?v=xnrXidwg83I>. Blood was collected

716 prior to the vaccine being administered (day 0), on the same day, and daily thereafter over
717 the next 10 days. This protocol was followed for both the priming and booster doses.

718 For serology applications, 20 μ l of blood was collected using a Mitra blood collection device
719 (Neoteryx, Torrance, CA, USA) prior to the vaccine being administered and on days 7 and 14
720 after vaccination with the priming and booster doses.

721 IMPROVISE Cohort: For the IMPROVISE study, samples were collected using PaxGene Blood
722 RNA tubes (BD Biosciences, Franklin Lakes, NJ, USA) at all timepoints and were frozen at -20C
723 until further processing.

724 PREDICT-19 Cohort: For the Italian cohort of the PREDICT-19 study, blood samples were
725 collected during hospitalization by venipuncture in tubes containing an RNA stabilizing
726 solution (Tempus™ Blood RNA Tube, ThermoFisher, Waltham, MA, USA, Catalog number:
727 4342792) and frozen at -20C until further processing.

728

729 **Multiplex serological assay**

730 The presence of antibodies against selected Human Coronaviruses proteins in the serum was
731 measured with a home-built bead array based on carboxymethylated beads sets with six
732 distinct intensities of a UV-excitable dye. Each bead set was individually coupled to 3 SARS-
733 CoV-2 proteins, envelope, nucleoprotein, Spike protein in its trimeric form-or its fragments,
734 and the S1 fragment of SARS-CoV S protein. Therefore, the complete array consisted of 6
735 antigens, including five SARS-CoV-2 antigens (Full Spike Trimer, Receptor Binding Domain,
736 Spike S1, Nucleoprotein, and Envelope), as well as the closely related SARS-CoV-S1 protein.
737 The binding of human antibodies to each viral antigen (bead set) is revealed with fluorescently
738 labeled isotype-specific mouse monoclonal or polyclonal antibodies. We measured total IgM,
739 total IgG, total IgA, as well as their individual isotypes, IgG1, IgG2, IgG3, IgA1, and IgA2,

740 reporting a total of 48 parameters per sample. The assays were performed on filter plates and
741 acquired on a BD-Symphony A5 using a high-throughput-sampler. An average of 300 beads
742 per region was acquired, and the median fluorescence intensity (MFI) for each isotype binding
743 was used for characterizing the antibody response. An antibody response index was
744 calculated as the ratio of the MFI of pooled negative blood controls collected prior to June
745 2018 (Sidra IRB 1609004823) to the MFI obtained for vaccinated donor samples.

746

747 **RNA extraction and QC**

748 RNA was extracted using the Tempus Spin RNA Isolation Kit (ThermoFisher), which was
749 adapted for the handling of small blood volumes. The methodology has been described
750 previously in detail (34). Contaminating DNA was removed using the TurboDNase kit
751 (ThermoFisher), and RNA was quantitated on a Qubit instrument (ThermoFisher) and QCed
752 using an Agilent 2100 Bioanalyzer (Agilent, Santa Clara, California, USA).

753

754 **RNA sequencing**

755 COVAX & IMPROVISE Cohorts: mRNA-sequencing was performed using QuantSeq 3' mRNA-
756 Seq Library Prep Kit FWD for Illumina (75 single-end) with a read depth of 8M and average
757 read alignment of 79.60%. Single samples were sequenced across four lanes, and the resulting
758 FASTQ files were merged by sample. Quality trimming is performed to remove adapter
759 sequences and polyA tails. Then trimmed reads were aligned to human genome
760 GRCh38/hg38 (Genome Reference Consortium Human Build 38), INSDC Assembly
761 GCA_000001405.28, Dec 2013) using STAR 2.6.1d and featureCounts v2.0.0 was used to
762 generate the raw counts. Raw expression data were normalized to size factor effects using R
763 package DESeq2. All downstream analyses were performed using R version 4.1 unless

764 otherwise specified. Global transcriptional differences between samples were assessed by
765 principal component analysis using the “prcomp” function. Transcriptome profiling data were
766 deposited, along with detailed sample information, into a public repository, the NCBI Gene
767 Expression Omnibus (GEO), with accession ID GSE190001 and BioProject ID: PRJNA785113
768 PREDICT-19 Cohort: Total RNA was isolated from whole blood lysate using the Tempus Spin
769 Isolation kit (Applied Biosystems) according to the manufacturer's instructions. Globin mRNA
770 was depleted from a portion of each total RNA sample using the GLOBINclear™-Human kit
771 (Thermo Fisher). Following the removal of globin transcripts transcriptome profiles were
772 generated via mRNA sequencing. Then mRNA-sequencing was performed using Illumina
773 HiSeq 4000 Technology (75 paired-end) with a read depth of 60M. Single samples were
774 sequenced across four lanes, resulting FASTQ files were merged by sample. All FASTQ passed
775 QC and were aligned to reference genome GRCh38 using STAR (2.6.1d). BAM files were
776 converted to a raw count's expression matrix using HTSeq (<https://github.com/Sydney->
777 [Informatics-Hub/RNASeq-DE](https://github.com/Sydney-Informatics-Hub/RNASeq-DE)). Raw count data was normalized using DESeq2. The ensemble
778 IDs targeting multiple genes were collapsed (average), and a final data matrix gene was
779 generated for modular repertoire analysis.

780

781 **Statistical Analysis**

782 Analyses were conducted using pre-defined gene sets. Specifically, we employed a fixed
783 repertoire of 382 transcriptional modules that were thoroughly functionally annotated, as
784 described in detail in a recent publication (10). Briefly, this repertoire of transcriptional
785 modules (“BloodGen3”) was identified based on co-expression, as measured in a collection of
786 16 blood transcriptome datasets encompassing 985 individual transcriptome profiles. Sets of
787 co-expressed transcripts were derived from the analysis of a large weighted co-clustering

788 network. Downstream analysis results and visualizations were generated employing a custom
789 R package (35). “Module response” is defined as the percentage of constitutive transcripts
790 with a given abundance that was determined to be different between two study groups, or
791 for the same individual in comparison to a given baseline (in this study, pre-vaccination
792 abundance levels). The values, therefore, ranged from 100% (all constitutive transcripts
793 increased) to -100% (all constitutive transcripts decreased). Only the dominant trend (i.e.,
794 increase or decrease in abundance over control/baseline) was retained for visualization
795 purposes on fingerprint grids or fingerprint heatmaps, with red indicating an increase and
796 blue a decrease in abundance. When performing group comparisons (e.g., cases vs controls
797 for the disease datasets used as reference), the p-value and false discovery rate cutoffs were
798 applied, which are mentioned in the figure legend. When performing longitudinal analyses,
799 the module response is determined by employing fixed fold-change and expression difference
800 cutoffs. Module response values obtained were used for data visualization. Significance was
801 determined for each module using the differential gene set enrichment function of the
802 dearseq R package (11).

803

804 **Definition of Interferon Response Transcriptional Phenotypes**

805 Study cohorts were stratified based on patterns of interferon response for two distinct
806 interferon signatures, defined as A28/S1 (comprising modules M8.3, M10.1 and M15.127)
807 and A28/S2 (comprising modules M13.17, M15.64, M15.86). For this, phenotypes were
808 defined based on levels of response observed for these two “traits”, as follows:

809 Percentage response of the six IFN modules were scored base on degree of response (%
810 response ≥ 50 ; score = 2, $0 < \%$ response < 50 ; score =1 and ($\%$ response ≤ -50 ; score = -2, -
811 $50 < \%$ response < 0 ; score =-1). Then the average scores of S1(“M8.3”, “M10.1” and

812 "M15.127") and S2 ("M13.17" , "M15.64" , "M15.86") and phenotypes were classified using
813 cutoff at S1/S2++ (avg score ≥ 1), S1/S2+($1 < \text{avg score} < 0.33$), S1/S2($0.33 < \text{avg score} \leq$
814 0), and S1/S2 – (avg score < 0). The phenotypes were grouped as:

- 815 - "Interferon Response Transcriptional phenotypes I" = "IRTP I" =
816 "A28/S1++A28/S2+", "A28/S1++A28/S20", "A28/S1+A28/S2+",
- 817 - "IRTP II" = A28/S1++A28/S2++",
- 818 - "IRTP III" = "A28/S1-A28/S2++", "A28/S1-A28/S2+", "A28/S10A28/S2++",
819 "A28/S10A28/S2+", "A28/S1-A28/S20"
- 820 - The "other " category encompassed the less prevalent phenotypes remaining =
821 "A28/S1+A28/S20", "A28/S10A8/S2+", "A8/S1+A28/S2", "A28/S10A28/S20",
822 "A28/S10A28/S2-", "A28/S1-A28/S2-", "A28/S1+A28/S2++"

823

824 **ACKNOWLEDGMENTS:**

825 We wish to acknowledge Michelle Esblaca and Juvilyn Gusi for their assistance with the
826 training of subjects and collection of blood samples, as well as the research subjects for
827 volunteering and making the study possible.

828

829 **AUTHOR CONTRIBUTION**

830 Conceptualization, D.R., S.D., D.B., J-C.G., and D.C.; Methodology, D.R., S.D., B.K., I.P., S.M.,
831 G.G., D.B., J-C.G., and D.C.; Data Generation, D.R., S.D., G.Z., B.K., S.T., I.P., S.M., G.G., L.M.,
832 L.L., F-R.V., G.M., S.L., T.C., M.S., R.B., S.Z., A.DM., B.T., A. AH., D.B., J-C.G., and D.C.;
833 Investigation, D.R., S.D., G.Z., D.B., J-C.G., and D.C.; Resources, D.R., S.D., G.Z., I.S., G.C., C.D.,
834 P.Cu., D.R.G., F.B., A.G., B.C., P.Cr., T.A., N.V., M. Be., A.B., M.Ba., S.Z., A.DM., B.T., A. AH.,
835 D.B., J-C.G., and D.C.; Formal Analysis, D.R., S.D., B.K., I.P., S.M., G.G., M.T., L.M., L.L., F-R.V.,

836 G.M., S.L., B. H., R.T., T.C., M.S., D.B., J-C.G., and D.C.; Patient Enrollment and Follow up, G.Z.,
837 S.T., I.S., G.C., C.D., P.Cu., D.R.G., F.B., A.G., B.C., P.Cr., M. Be., A.B., M.Ba., T.A., R.B., S.Z.,
838 A.DM., B.T., A. AH., Writing - Original Draft, D.R., S.D., G.G., D.B., J-C.G., and D.C.; Writing -
839 Review & Editing, all authors; Visualization, D.R., S.D., B. H., R.T., and D.C.; Supervision, D.R.,
840 S.D., G.Z., S.L., K.S., S.Z., A.DM., B.T., A. AH., D.B., J-C.G., and D.C.;

841

842 **COMPETING INTERESTS STATEMENT**

843 D.R.G. outside of this work, reports investigator-initiated grants from Gilead Italia and Pfizer
844 Inc. M.Ba Outside of this work work, reports research grants and/or advisor/consultant
845 and/or Speaker/chairman Bayer, Biomerieux, Cidara, Cipla, Gilead, Menarini, MSD, Pfizer,
846 Shionogi". The other authors have no competing interests to report.

847

848 **REFERENCES**

- 849 1. Tregoning JS, Flight KE, Higham SL, Wang Z, Pierce BF. Progress of the COVID-19 vaccine
850 effort: viruses, vaccines and variants versus efficacy, effectiveness and escape. *Nat Rev*
851 *Immunol.* 2021 Aug 9;
- 852 2. Gaucher D, Therrien R, Kettaf N, Angermann BR, Boucher G, Filali-Mouhim A, et al.
853 Yellow fever vaccine induces integrated multilineage and polyfunctional immune
854 responses. *J Exp Med.* 2008 Dec 22;205(13):3119–31.
- 855 3. Querec TD, Akondy RS, Lee EK, Cao W, Nakaya HI, Teuwen D, et al. Systems biology
856 approach predicts immunogenicity of the yellow fever vaccine in humans. *Nat*
857 *Immunol.* 2009 Jan;10(1):116–25.
- 858 4. Hagan T, Nakaya HI, Subramaniam S, Pulendran B. Systems vaccinology: Enabling
859 rational vaccine design with systems biological approaches. *Vaccine.* 2015 Sep
860 29;33(40):5294–301.
- 861 5. Arunachalam PS, Scott MKD, Hagan T, Li C, Feng Y, Wimmers F, et al. Systems
862 vaccinology of the BNT162b2 mRNA vaccine in humans. *Nature.* 2021 Jul 12;
- 863 6. Obermoser G, Presnell S, Domico K, Xu H, Wang Y, Anguiano E, et al. Systems scale
864 interactive exploration reveals quantitative and qualitative differences in response to
865 influenza and pneumococcal vaccines. *Immunity.* 2013 Apr 18;38(4):831–44.

- 866 7. Rinchai D, Anguiano E, Nguyen P, Chaussabel D. Finger stick blood collection for gene
867 expression profiling and storage of tempus blood RNA tubes. *F1000Res*. 2016;5:1385.
- 868 8. Hadjadj J, Yatim N, Barnabei L, Corneau A, Boussier J, Smith N, et al. Impaired type I
869 interferon activity and inflammatory responses in severe COVID-19 patients. *Science*.
870 2020 Aug 7;369(6504):718–24.
- 871 9. De Mot L, Bechtold V, Bol V, Callegaro A, Coccia M, Essaghir A, et al. Transcriptional
872 profiles of adjuvanted hepatitis B vaccines display variable interindividual homogeneity
873 but a shared core signature. *Sci Transl Med*. 2020 Nov 11;12(569):eaay8618.
- 874 10. Altman MC, Rinchai D, Baldwin N, Toufiq M, Whalen E, Garand M, et al. Development of
875 a fixed module repertoire for the analysis and interpretation of blood transcriptome
876 data. *Nat Commun*. 2021 Jul 19;12(1):4385.
- 877 11. Agniel D, Hejblum BP. Variance component score test for time-course gene set analysis
878 of longitudinal RNA-seq data. *Biostatistics*. 2017 Oct 1;18(4):589–604.
- 879 12. Rawat A, Rinchai D, Toufiq M, Marr AK, Kino T, Garand M, et al. A Neutrophil-Driven
880 Inflammatory Signature Characterizes the Blood Transcriptome Fingerprint of Psoriasis.
881 *Front Immunol* [Internet]. 2020 [cited 2020 Dec 7];11. Available from:
882 <https://www.frontiersin.org/articles/10.3389/fimmu.2020.587946/full>
- 883 13. Sena LA, Li S, Jairaman A, Prakriya M, Ezponda T, Hildeman DA, et al. Mitochondria Are
884 Required for Antigen-Specific T Cell Activation through Reactive Oxygen Species
885 Signaling. *Immunity*. 2013 Feb 21;38(2):225–36.
- 886 14. Nakaya HI, Wrammert J, Lee EK, Racioppi L, Marie-Kunze S, Haining WN, et al. Systems
887 biology of vaccination for seasonal influenza in humans. *Nat Immunol*. 2011 Jul
888 10;12(8):786–95.
- 889 15. Nakaya HI, Hagan T, Duraisingham SS, Lee EK, Kwissa M, Rouphael N, et al. Systems
890 Analysis of Immunity to Influenza Vaccination across Multiple Years and in Diverse
891 Populations Reveals Shared Molecular Signatures. *Immunity*. 2015 Dec 15;43(6):1186–
892 98.
- 893 16. Rinchai D, Altman MC, Konza O, Hässler S, Martina F, Toufiq M, et al. Definition of
894 erythroid cell-positive blood transcriptome phenotypes associated with severe
895 respiratory syncytial virus infection. *Clinical and Translational Medicine*.
896 2020;10(8):e244.
- 897 17. Tang B, Shojaei M, Wang Y, Nalos M, Mclean A, Afrasiabi A, et al. Prospective validation
898 study of prognostic biomarkers to predict adverse outcomes in patients with COVID-
899 19: a study protocol. *BMJ Open*. 2021 Jan 6;11(1):e044497.
- 900 18. Elahi S. Neglected Cells: Immunomodulatory Roles of CD71+ Erythroid Cells. *Trends*
901 *Immunol*. 2019 Mar;40(3):181–5.

- 902 19. Elahi S, Ertelt JM, Kinder JM, Jiang TT, Zhang X, Xin L, et al. Immunosuppressive CD71+
903 erythroid cells compromise neonatal host defence against infection. *Nature*. 2013 Dec
904 5;504(7478):158–62.
- 905 20. Shahbaz S, Xu L, Osman M, Sligl W, Shields J, Joyce M, et al. Erythroid precursors and
906 progenitors suppress adaptive immunity and get invaded by SARS-CoV-2. *Stem Cell*
907 *Reports*. 2021 May 11;16(5):1165–81.
- 908 21. Spann KM, Tran K-C, Chi B, Rabin RL, Collins PL. Suppression of the induction of alpha,
909 beta, and lambda interferons by the NS1 and NS2 proteins of human respiratory
910 syncytial virus in human epithelial cells and macrophages [corrected]. *J Virol*. 2004
911 Apr;78(8):4363–9.
- 912 22. Bossert B, Conzelmann K-K. Respiratory syncytial virus (RSV) nonstructural (NS) proteins
913 as host range determinants: a chimeric bovine RSV with NS genes from human RSV is
914 attenuated in interferon-competent bovine cells. *J Virol*. 2002 May;76(9):4287–93.
- 915 23. Singer M, Deutschman CS, Seymour CW, Shankar-Hari M, Annane D, Bauer M, et al. The
916 Third International Consensus Definitions for Sepsis and Septic Shock (Sepsis-3). *JAMA*.
917 2016 Feb 23;315(8):801–10.
- 918 24. Chiche L, Jourde-Chiche N, Whalen E, Presnell S, Gersuk V, Dang K, et al. Modular
919 transcriptional repertoire analyses of adults with systemic lupus erythematosus reveal
920 distinct type I and type II interferon signatures. *Arthritis & Rheumatology (Hoboken,*
921 *NJ)*. 2014 Jun;66(6):1583–95.
- 922 25. Galani I-E, Rovina N, Lampropoulou V, Triantafyllia V, Manioudaki M, Pavlos E, et al.
923 Untuned antiviral immunity in COVID-19 revealed by temporal type I/III interferon
924 patterns and flu comparison. *Nat Immunol*. 2021 Jan;22(1):32–40.
- 925 26. Zhang Q, Bastard P, Liu Z, Le Pen J, Moncada-Velez M, Chen J, et al. Inborn errors of type
926 I IFN immunity in patients with life-threatening COVID-19. *Science*. 2020 Oct
927 23;370(6515):eabd4570.
- 928 27. Bastard P, Rosen LB, Zhang Q, Michailidis E, Hoffmann H-H, Zhang Y, et al.
929 Autoantibodies against type I IFNs in patients with life-threatening COVID-19. *Science*.
930 2020 Oct 23;370(6515):eabd4585.
- 931 28. Bastard P, Gervais A, Le Voyer T, Rosain J, Philippot Q, Manry J, et al. Autoantibodies
932 neutralizing type I IFNs are present in ~4% of uninfected individuals over 70 years old
933 and account for ~20% of COVID-19 deaths. *Sci Immunol*. 2021 Aug 19;6(62):eabl4340.
- 934 29. Cheng H, Peng Z, Luo W, Si S, Mo M, Zhou H, et al. Efficacy and Safety of COVID-19
935 Vaccines in Phase III Trials: A Meta-Analysis. *Vaccines*. 2021 Jun;9(6):582.
- 936 30. Mulligan MJ, Lyke KE, Kitchin N, Absalon J, Gurtman A, Lockhart S, et al. Phase I/II study
937 of COVID-19 RNA vaccine BNT162b1 in adults. *Nature*. 2020 Oct;586(7830):589–93.

- 938 31. Milanez-Almeida P, Martins AJ, Germain RN, Tsang JS. Cancer prognosis with shallow
939 tumor RNA sequencing. *Nat Med.* 2020 Feb;26(2):188–92.
- 940 32. Haack AJ, Lim FY, Kennedy DS, Day JH, Adams KN, Lee JJ, et al. homeRNA: A self-
941 sampling kit for the collection of peripheral blood and stabilization of RNA [Internet].
942 2021 Feb [cited 2021 Oct 30] p. 2021.02.08.430337. Available from:
943 <https://www.biorxiv.org/content/10.1101/2021.02.08.430337v1>
- 944 33. Sadarangani M, Marchant A, Kollmann TR. Immunological mechanisms of vaccine-
945 induced protection against COVID-19 in humans. *Nat Rev Immunol.* 2021
946 Aug;21(8):475–84.
- 947 34. Syed Ahamed Kabeer B, Tomei S, Mattei V, Brummaier T, McGready R, Nosten F, et al. A
948 protocol for extraction of total RNA from finger stick whole blood samples preserved
949 with Tempus™ solution. *F1000Res.* 2018 Nov 2;7:1739.
- 950 35. Rinchai D, Roelands J, Toufiq M, Hendrickx W, Altman MC, Bedognetti D, et al.
951 BloodGen3Module: Blood transcriptional module repertoire analysis and visualization
952 using R. *Bioinformatics.* 2021 Feb 24;
- 953
- 954
- 955
- 956
- 957
- 958
- 959
- 960
- 961
- 962
- 963
- 964
- 965
- 966

967 **Table 1: Subject characteristics**

Patient ID	Vaccine name	Gender	Age	Ethnicity	Previous COVID-19	Underlying disease	Drugs	Symptoms at prime (Type)	Symptoms at prime (Grade)	Symptoms at boost (Type)	Symptoms at boost (Grade)
PZB1	Pfizer Biontech	Female	38	Asian	Yes	No	no	Myalgia	G1	Fever/Myalgia	G1
PZB2	Pfizer Biontech	Male	47	Caucasian	Yes	No	no	Myalgia	G1	Myalgia	G1
PZB3	Pfizer Biontech	Male	57	Caucasian	Yes	T2D	Metformin, Insulin	Myalgia	G1	Myalgia	G1
PZB4	Pfizer Biontech	Female	34	Indian	No	No	no	None	NA	Chills/Insomnia/Headache/Myalgia/Fatigue	G3
PZB5	Pfizer Biontech	Male	38	Indian	No	No	no	Myalgia	G1	Myalgia	G1
PZB6	Pfizer Biontech	Female	48	Caucasian	No	No	no	Myalgia/Headache	G1	Myalgia	G1
PZB7	Pfizer Biontech	Female	34	Caucasia/Arab	No	Hashimoto thyroiditis	no	None	NA	None	NA
PZB8	Pfizer Biontech	Female	29	Arab	No	No	no	Myalgia/Swelling	G1	Fever/Myalgia	G1
PZB9	Pfizer Biontech	Male	41	Arab	No	Allergic rhinitis	no	Myalgia	G1	Myalgia	G1
PZB10	Pfizer Biontech	Female	35	Arab	No	No	no	Myalgia	G1	Fever/Insomnia/Myalgia/Fatigue	G2
PZB11	Pfizer Biontech	Male	41	Caucasian	No	No	no	Myalgia	G2	Myalgia	G1
PZB12	Pfizer Biontech	Female	34	Indian	No	Hypothyroidism	Levothyroxine	None	NA	Fever/Myalgia	G1
PZB13	Pfizer Biontech	Male	29	Indian	No	No	no	Fatigue	G1	Fever/Heaviness in arm	G2
PZB14	Pfizer Biontech	Female	38	Arab	No	Allergic	no	Myalgia/Headache	G1	Fatigue	G1
PZB15	Pfizer Biontech	Male	43	Arab	No	Hypothyroidism	Levothyroxine	None	NA	Myalgia/Headache	G2
PZB16	Pfizer Biontech	Female	39	Indian	No	No	no	Heaviness in arm	G1	Fever/Myalgia/Fatigue	G2
PZB17	Pfizer Biontech	Female	42	Indian	Yes	T2D, Hypertension	Methformin, Telmisartan	Fever/Headache/Myalgia/Fatigue	G2	Fatigue/Gastritis	G2
MDA18	Moderna	Male	42	Caucasian	No	Hypertension	Amlodipine, Ramipril	Myalgia	G1	Myalgia	G1
PZB19	Pfizer Biontech	Female	39	Caucasian	No	No	no	Myalgia	G1	Headache/Myalgia/Arthralgia	G3
MDA20	Moderna	Female	36	Arab	Yes	No	no	Chills/Myalgia	G2	Chills/Myalgia	G2
MDA21	Moderna	Female	36	Caucasian	No	No	no	Myalgia	G1	Fever/Skin rash/Myalgia	G2
PZB25	Pfizer Biontech	Female	39	Caucasian	No	No	no	Myalgia	G1	Myalgia	G1

MDA26	Moderna	Female	30	Caucasian	Yes	Asthma	Sereti de, Salbut amol	Fever/Head ache/Myalgi a/Fatigue	G3	Asthma attack/Fever /Myalgia/Fati gue	G3
-------	---------	--------	----	-----------	-----	--------	---------------------------------	--	----	--	----

Footnotes:

T2D: Type 2 Diabetes

Vaccine type and lot, and subjects' characteristics were recorded, including demographic, biometric data, blood group, underlying diseases, drugs usage, and previous COVID-19 disease.

Every subject recorded and graded the symptoms that occurred after the first and second vaccinations doses, according to the NIH "DAIDS AE Grading Table"

968

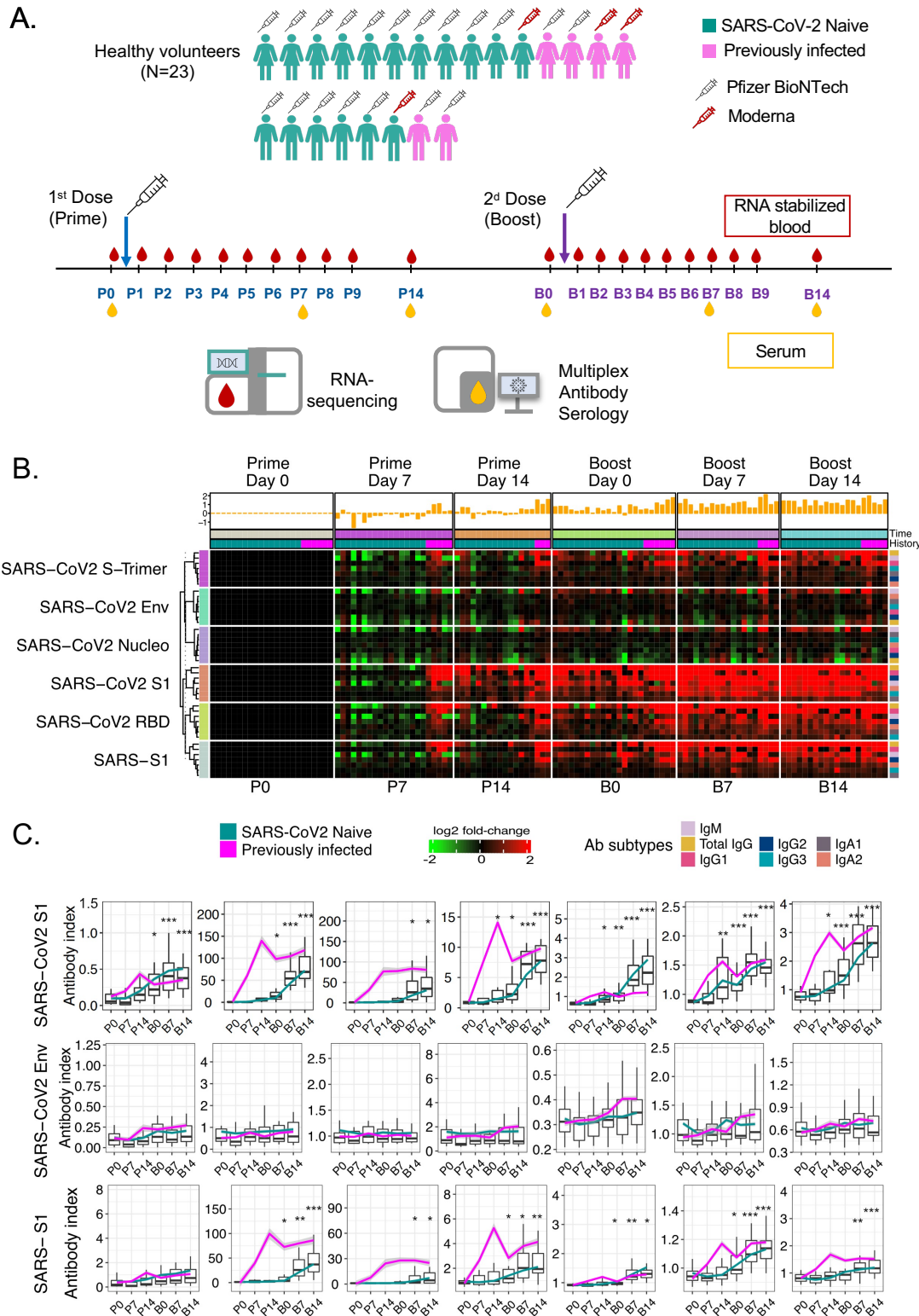


Figure 1: Antibody response to COVID-19 mRNA vaccination. (A) Schematic representation of the study design. (B) The heatmap represents changes in abundance of antibodies specific to several SARS-CoV-2 antigens and control antigens relative to pre-vaccination levels. Red indicates a relative increase, and green indicates a relative decrease in abundance. Columns represent subjects arranged by timepoint and have colored tracks at the top indicating whether the subjects were previously infected with SARS-CoV-2 or not. The histogram above represents the average log₂ fold-change over baseline for a given column. The rows represent antibody reactivities arranged by antigen specificity. The different rows represent the isotypes of reactive antibodies, arranged according to the color legend specified below the heat map. (C) Changes in antibody levels expressed as an “antibody index” are shown on the box plots, each corresponding to a given antibody type of a given specificity. Lines indicate changes for individuals previously infected with SARS-CoV-2 and who had recovered (in pink) and for naïve individuals (in green). Centerlines, box limits, and whiskers represent the median, interquartile range, and 1.5x interquartile range, respectively. Multiple pairwise tests (paired t-test) were performed comparing antibodies levels to baseline (D0). Asterisks: * represent $p < .01$, **represent $p < .001$, *** represent $p < .0001$.

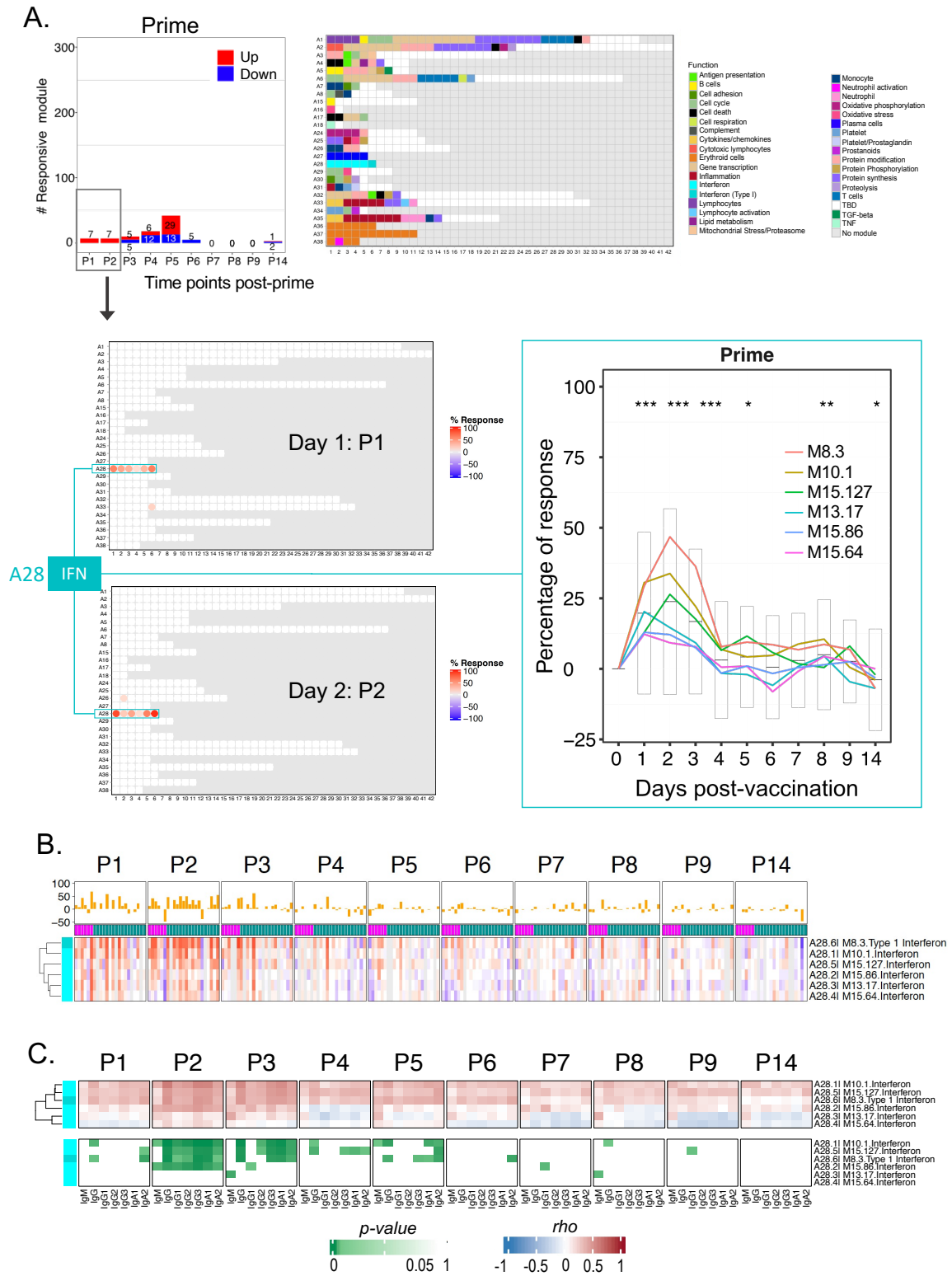


Figure 2: Characterization of the post-prime interferon response signature. (A) The bar graph shows the cumulative module response at the various timepoints following the administration of the priming dose of the vaccine (noted P1-P14). The Y-axis values and numbers on the bars indicate the number of modules meeting the 15% response threshold (out of a total of 382 modules constituting the BloodGen3 repertoire, with percentage response corresponding to the proportion of transcripts predominantly increased or decreased compared to baseline using FDR < 0.1 as the cutoff to determine significance [DESeq2]). The number of modules for which abundance was predominantly increased is shown in red, and those for which abundance was predominantly decreased are shown in blue. The fingerprint grid plots represent the overall module responses on day 1 post-prime (P1) and day 2 post-prime (P2). Modules from the BloodGen3 repertoire occupy fixed positions on the fingerprint grids. They are arranged as rows based on membership to module aggregates (rows A1 through A38). Changes compared to the pre-vaccination baseline are indicated on the grid by red and blue spots of varying color intensity, which indicate the “percentage response” for a given module. The color key at the top indicates the various functions attributed

to the modules that are represented on the grid. The response of the six modules comprising aggregate A28 is represented on a line graph that shows the proportion of responsive transcripts for each module across all the post-prime timepoints. For each module, the statistical significance of the overall response was determined by time-course gene set enrichment analysis. Four of the six A28 modules met significance thresholds $FDR < 0.1$ (M8.3: p-value = 1.9×10^{-4} , $FDR = 0.019$, M10.1: p-value = 1.9×10^{-4} , $FDR = 0.019$, M15.127: p-value = 1.9×10^{-4} , $FDR = 0.019$, 727 and M15.86: p-value = 3.9×10^{-4} , $FDR = 0.031$) and all six A28 modules $p < 0.05$ (M13.17: p-value = 1.5×10^{-3} , $FDR = 0.101$ and M15.64: p-value = 0.044, $FDR = 0.727$). We also ascertained the significance of changes measured post-prime at the level of this module aggregate and at each time point (paired t-test comparing module response at each time point relative to the pre-vaccination baseline; * $p < 0.01$, ** $p < 0.001$, *** $p < 0.0001$). (B) Heatmaps represent proportions of transcripts that changed within the six A28 modules at different timepoints and across different individuals compared to pre-vaccination baseline values. Red indicates that transcripts were predominantly increased over the baseline, and blue indicates that transcripts were predominantly decreased. Rows represent the six A28 modules arranged within an aggregate via hierarchical clustering. Columns represent samples grouped by timepoint and show profiles of individual subjects within each timepoint. (C) The heatmaps represent associations (Spearman correlation test) between antibody responses measured 14 days after administration of COVID-19 booster doses and transcriptional responses measured across nine consecutive days after the priming dose. The heatmap at the top provides the correlation coefficients across multiple days and for each day across multiple subjects, with rows corresponding to the six A28 interferon modules. The heatmap below shows the significance of the correlations shown on the heatmap directly above, with the same ordering of rows and columns.

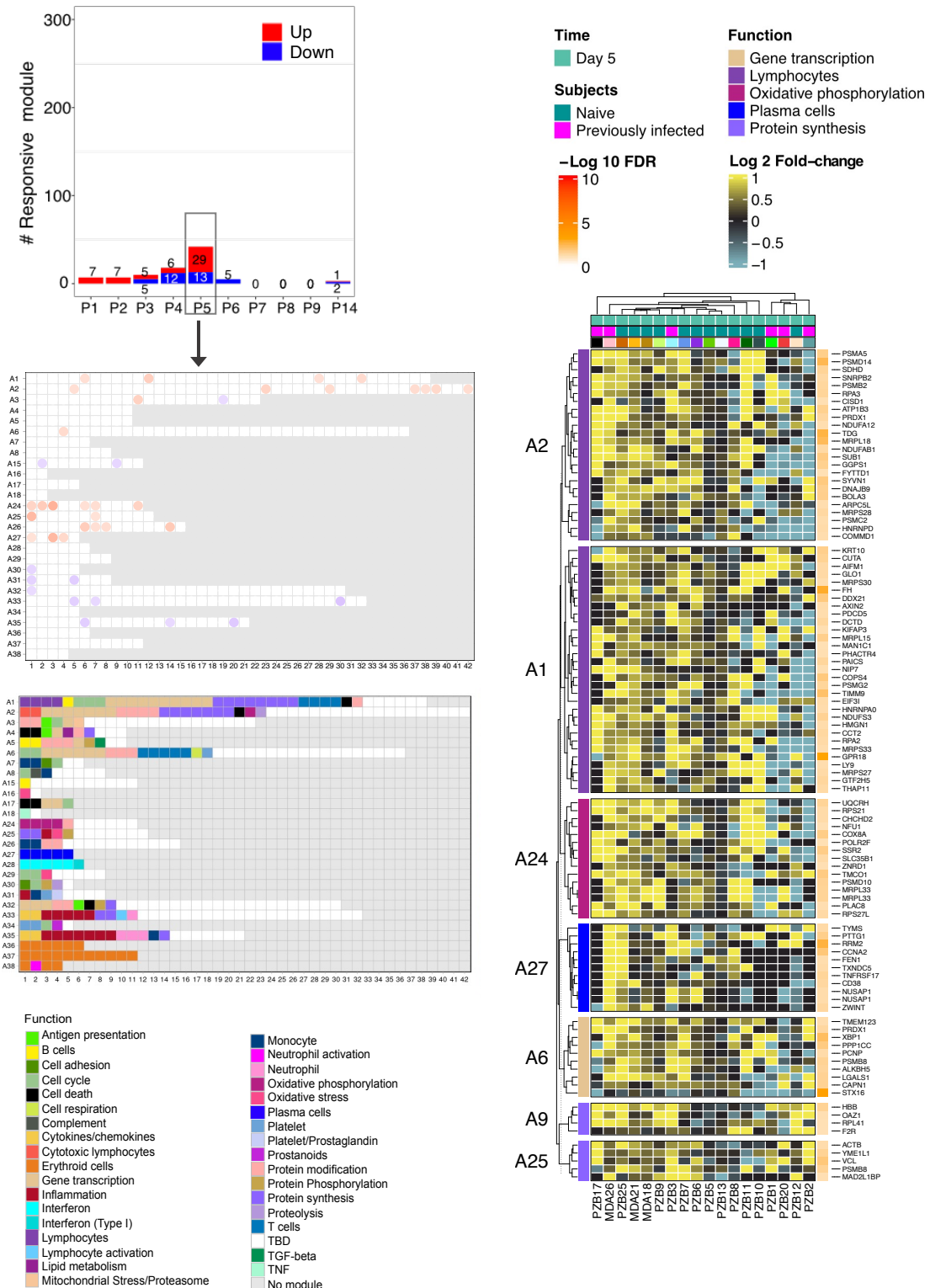


Figure 3: Characterization of responses on day 5 post-prime. (A) The bar graph shows the cumulative number of responsive modules at each timepoint following the administration of the priming dose of the vaccine (noted P1-P14). The fingerprint grid plot shows changes observed at P5 (day 5 post-prime). The position of the modules on the grid is fixed. The percent response of individual modules is represented on the grid by red and blue spots of varying color intensity denoting a predominant increase or decrease in abundance, respectively. The percentage response of a given module corresponds to the proportion of transcripts predominantly increased or decreased compared to baseline, meeting a significance cutoff of FDR < 0.1. The color key at the top indicates the various functions attributed to the modules that are represented on the grid. (B) The heatmap represents Log₂ average fold change in abundance of transcripts constituting sets of modules associated with given functional annotations on P5. Rows represent individual transcripts grouped according to the module aggregate they originate from, corresponding to the different rows on the fingerprint grid plot on the left. Each module aggregate is associated with a unique function, as indicated by the color key above. The columns on the heatmap represent individual subjects coded with the type of vaccine received (Pfizer BioNtech = PZB; Moderna = MDA).

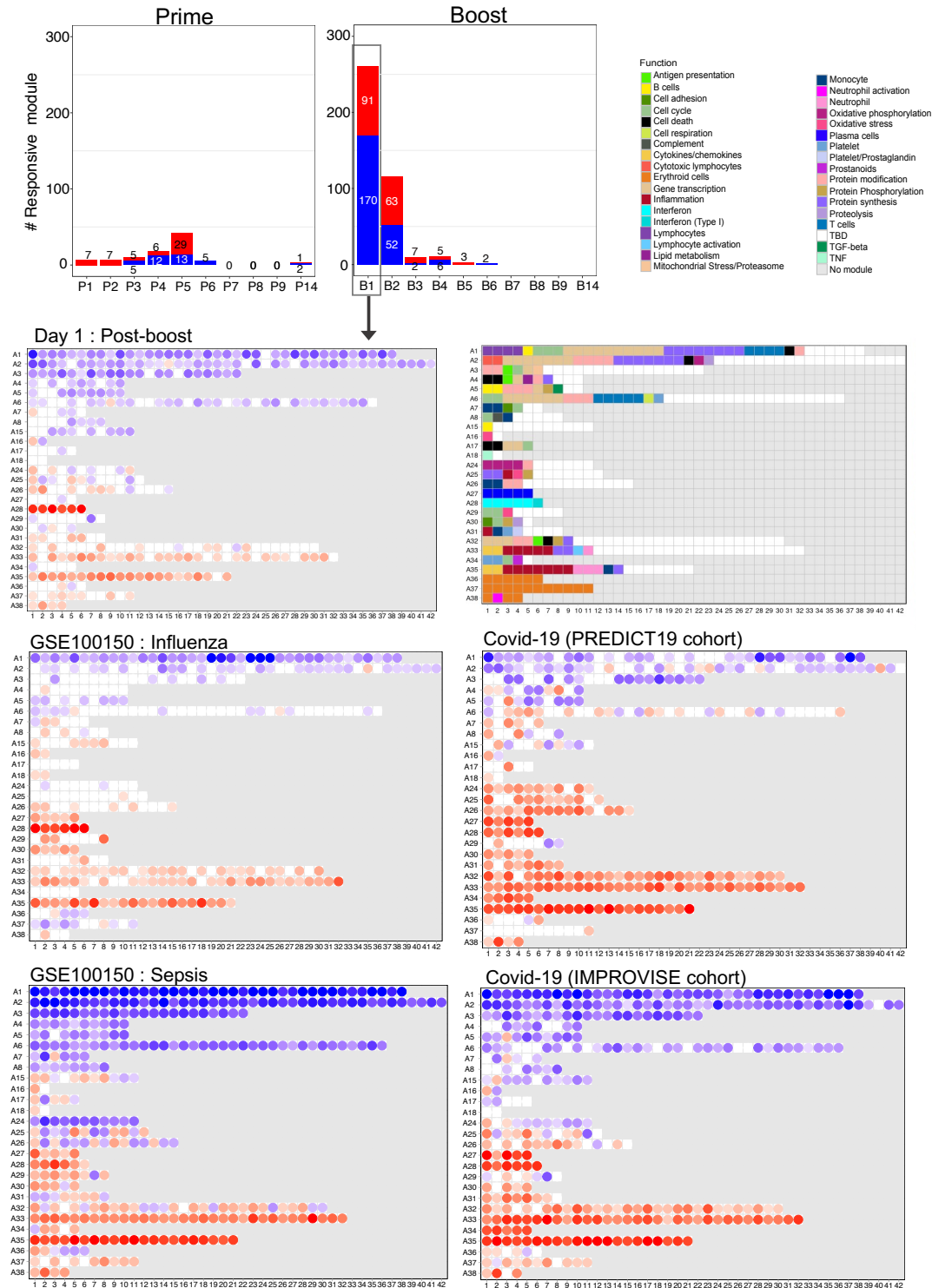
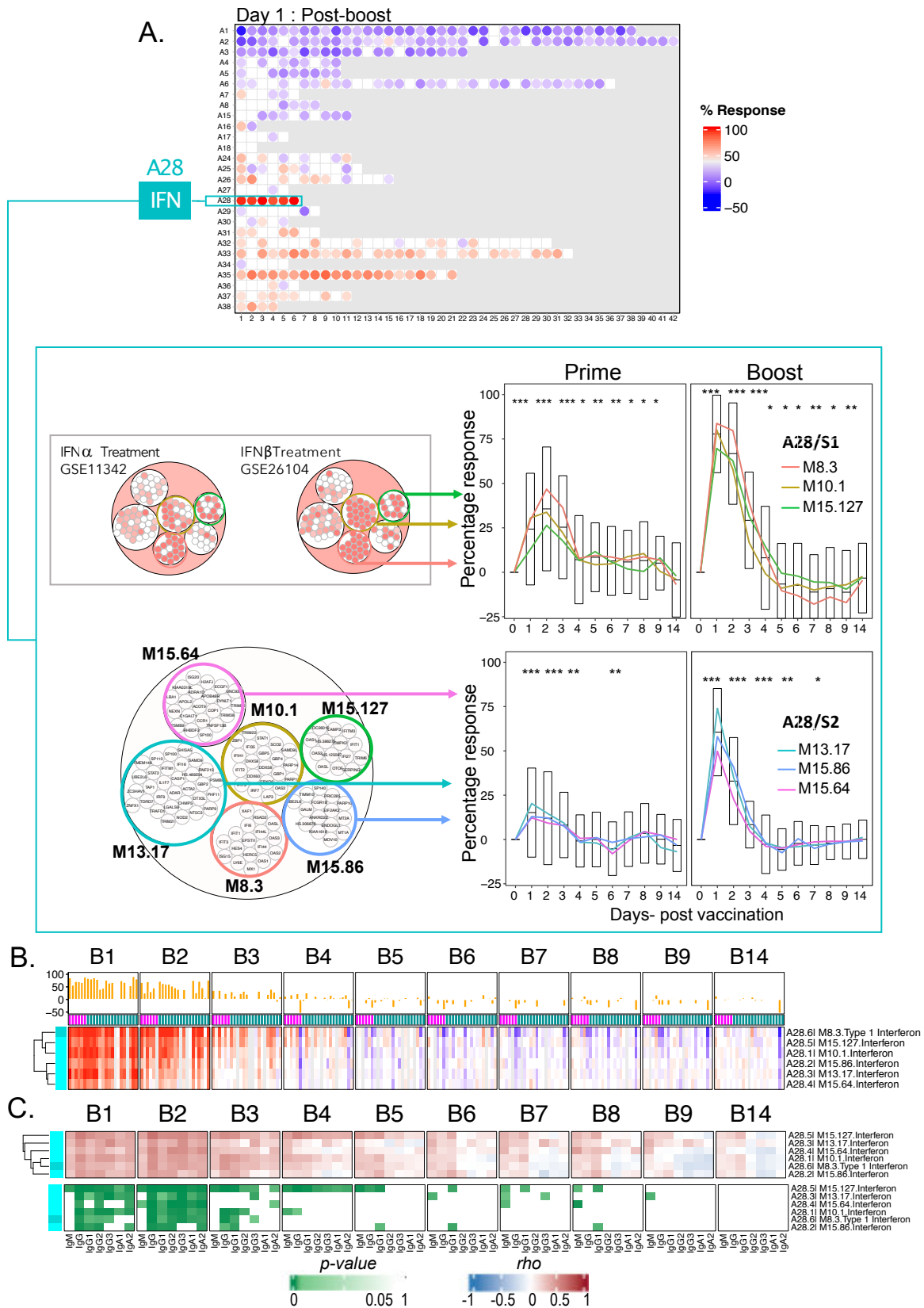


Figure 4: Fingerprint grid plots mapping changes observed on day 1 post-boost and across reference datasets.

The bar graphs show the cumulative module response at the various timepoints post-priming and booster doses (noted P1-P14 and B1-B14, respectively). The Y-axis values and numbers on the bars indicate the number of modules meeting the 15% response threshold (out of a total of 382 modules constituting the BloodGen3 repertoire, with percentage response corresponding to the proportion of transcripts predominantly increased or decreased compared to baseline meeting a significance cutoff of DESeq2, FDR < 0.1). The fingerprint grid plots show changes in transcript abundance in a given study group in comparison to baseline (pre-vaccination sample or uninfected control group – with the percent response of individual modules shown by red and blue spots of varying color intensity denoting predominant increase or decrease in abundance, respectively). Changes are shown in the top grid for a group comparison of 1 day after receiving the booster dose of COVID-19 mRNA vaccines with baseline pre-vaccination samples (this study). Grids in the middle and bottom positions show changes for patients with acute infections caused by influenza virus (public dataset) or SARS-CoV-2 (this study) and for patients with bacterial sepsis (public dataset). The color key at the top indicates the various functions attributed to the modules that occupy a fixed position on the grid plot.



value = 1.9-e4, FDR = 3.6-e4, M10.1: p-value = 1.9-e4, FDR = 3.6-e4, M13.17: p-value = 1.9-e4, FDR = 3.6-e4, M15.127: p-value = 1.9-e4, FDR = 3.6-e4, M15.64: p-value = 1.9-e4, FDR = 3.6-e4 and M15.86: p-value = 1.9-e4, FDR = 3.6-e4). In addition, we ascertained the significance of changes measured post-prime at the level of this module aggregate and at each time point (paired t-test comparing module response at each time point relative to the pre-vaccination baseline; * $p < 0.01$, ** $p < 0.001$, *** $p < 0.0001$). The circle packing plots on the left show module responses at the individual transcript level for two public blood transcriptome datasets. The larger circle below indicates official symbols for the individual transcripts. It also highlights the modules included in A28/S2, shown directly on the right. The smaller circles above show changes in abundance of A28 transcripts for two public datasets. One study (GSE11342) measured blood transcriptional response in patients with Hepatitis C infection treated with alpha-interferon (23). The second study (GSE26104) measured transcriptional response in subjects with multiple sclerosis treated with beta-interferon (24). A red circle indicates a significant increase in the abundance of transcripts compared to the pre-treatment baseline (* $|\text{fold-change}| > 1.5$, $\text{FDR} < 0.1$). **(B)** Changes in abundance compared to baseline pre-vaccination levels are represented on a heatmap, with modules as rows and individual samples as columns. The modules are arranged by hierarchical clustering based on abundance patterns across samples. The samples are arranged by timepoints post-prime (top) and post-boost (bottom). **(C)** The heatmaps represent associations (Spearman correlation) between antibody responses measured 14 days after administration of COVID-19 booster doses and transcriptional responses measured across nine consecutive days after the booster dose. The heatmap on top provides the correlation coefficients across multiple days and for each day across multiple subjects, with rows corresponding to the six A28 interferon modules. The heatmap below shows the significance of the correlations shown on the heatmap on top, with the same ordering of rows and columns.

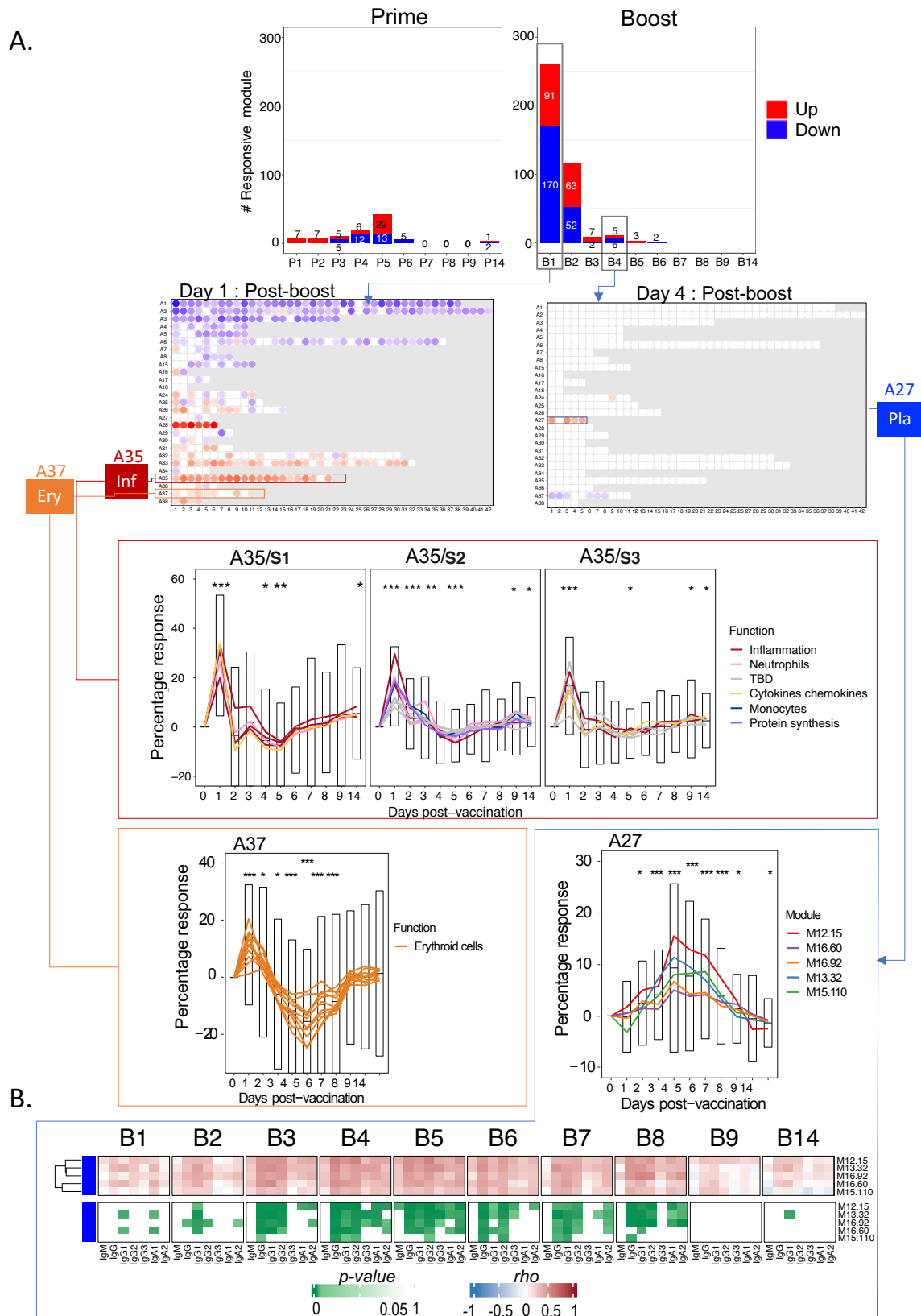


Figure 6: Characterization of post-booster inflammation, erythroid cell, and plasmablast responses. (A) The bar graph at the top represents the number of response modules at any given time point post-prime and post-boost. The fingerprint grid plots show the modules that had changes compared with a fixed visualization and interpretation framework. Changes are shown for the day 1 post-boost timepoint (left) as well as day 5 (right) (percent response is determined based on statistical cutoff: DESeq2, FRD < 0.1). On the left grid, modules belonging to aggregates A35 (associated with inflammation) and A37 (associated with erythroid cells) are highlighted. The profiles of those modules are represented on the line graphs below, which show the average percentage responses of A35 and A37 modules across multiple timepoints. The percentage response for a given module is the proportion of its constitutive transcripts showing significant changes, ranging from 0% to 100% when transcripts were predominantly increased to 0% to -100% when transcripts were predominantly decreased. Each line represents the profile of the modules

constituting a given aggregate. Line graphs for A35 were split into three sets according to differences in clustering patterns (A35/S1, A35/S2, and A35/S3). On the right grid, modules belonging to aggregates A27 (associated with platelets) are highlighted. The corresponding line graph below represents the changes in abundance of A27 modules over time following administration of the second dose of vaccine. For each module, statistical significance for the overall response was determined by time course gene set enrichment analysis using the *dearseq* R package. For A35, 20 of 21 modules met significance thresholds (p -value < 0.05 and FDR < 0.01). It was also the case in 11 of 11 modules for A37 and 4 of 5 modules for A27 (**Supplementary file 4**). In addition, we ascertained the significance of changes measured post-prime at the level of this module aggregate and at each time point (paired t-test comparing module response at each time point relative to the pre-vaccination baseline; * $p < 0.01$, ** $p < 0.001$, *** $p < 0.0001$). **(B)**. The heatmaps represent associations between antibody responses measured 14 days after administration of COVID-19 booster doses and transcriptional responses measured across nine consecutive days after the booster dose. Specifically, the heatmap at the top represents the correlation coefficients across multiple days and for each day across multiple subjects, with rows corresponding to the five A27 plasmablast modules. The heatmap below shows the significance of the correlations shown on the heatmap at the top, with the same order of rows and columns.

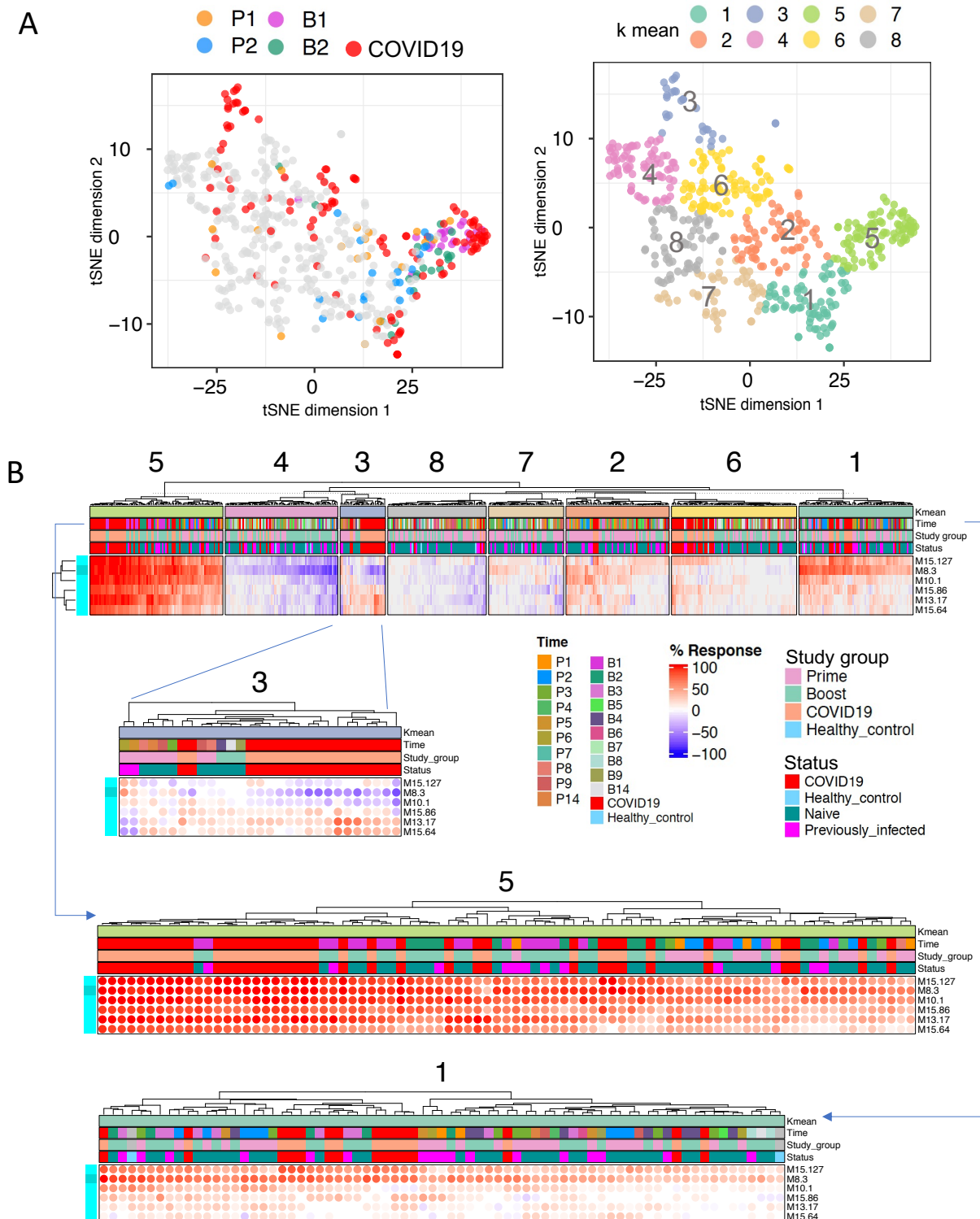


Figure 7: Comparing patterns of interferon response in vaccinated individuals and a cohort of COVID-19 patients. A. The tSNE plot represents similarities in patterns of interferon response induction across the six modules forming aggregate A28 and among samples comprised in our vaccination cohort and one of our COVID-19 disease cohorts (PREDICT-19 / Italy). COVID-19 samples are shown in red along with specific post-vaccination timepoints (post-prime days 1 and 2 [P1, P2], post-boost days 1 and 2 [B1, B2]). Samples from the consolidated cohorts were partitioned into 8 clusters via k-means clustering, the distribution of which is shown on the tSNE plot on the top right. **B.** Heatmaps show patterns of response for the six interferon response modules across the eight sample clusters. The red colors indicate that the abundance of transcripts for a given module is predominantly increased with the intensity representing the proportion of constitutive transcripts meeting a given threshold, which at the level of individual samples is a fixed fold change and difference cutoff ($|\text{Fold change}| > 1.5$, and $|\text{difference}| > 10$ in a given sample over its respective pre-vaccination baseline). The blue color denotes a predominant decrease in abundance of constitutive transcripts compared to the same individual's pre-vaccination baseline. Details are shown below for Clusters 3, 5, and 8 in separate heatmaps.

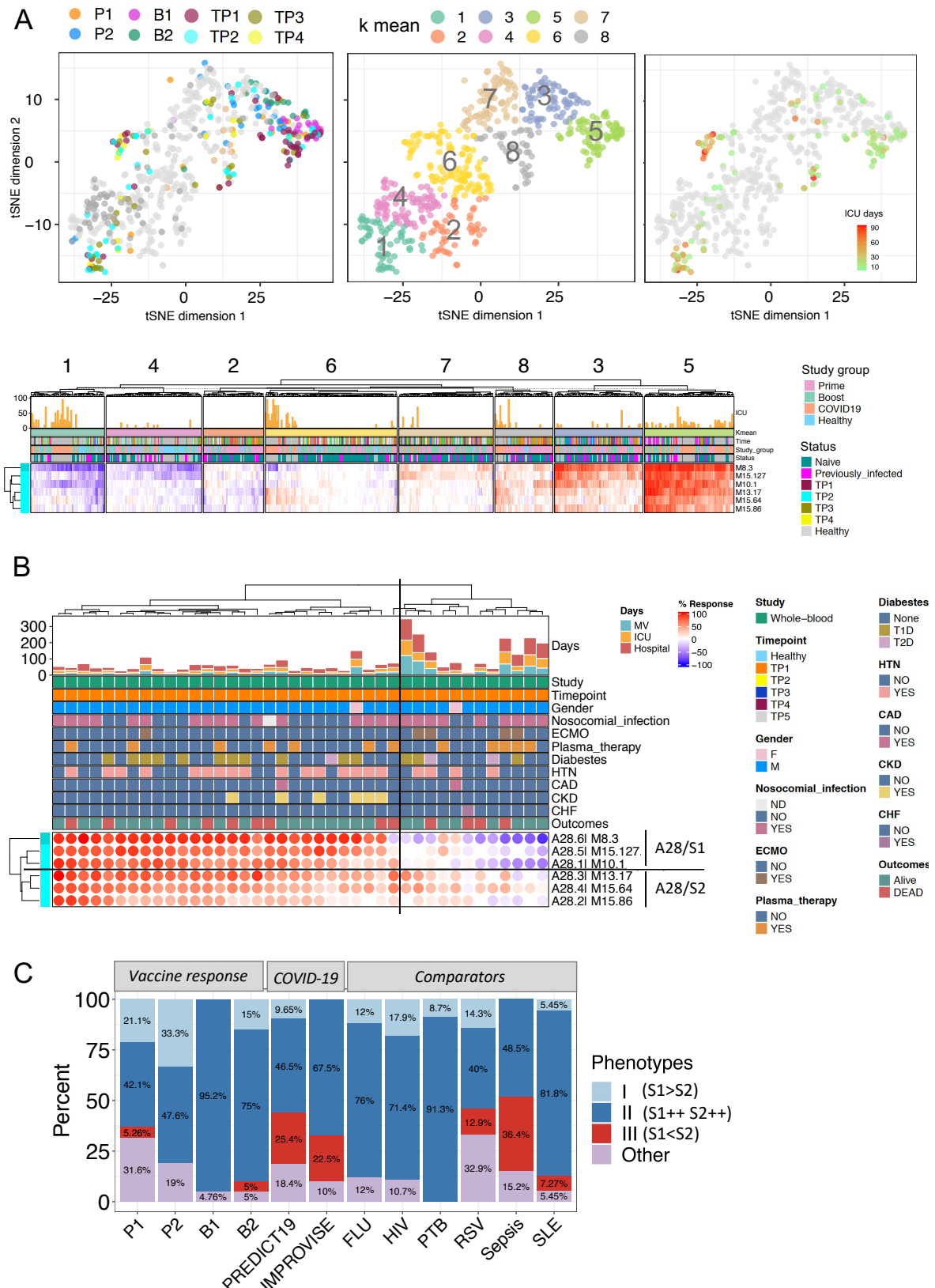


Figure 8: Comparison of interferon response patterns of vaccinated individuals and a cohort of COVID-19 patients with severe disease under intensive care. A. The tSNE plot represents similarities in patterns of interferon response induction across the six modules forming aggregate A28 and among samples comprised in our vaccination cohort and one of our COVID-19 disease cohorts (IMPROVISE). Specific post-vaccination timepoints (post-prime days 1 and 2 [P1, P2], post-boost days 1 and 2 [B1, B2]), as well as repeat sampling for COVID-19 patient (TP1, TP2, TP3, TP4, all collected during ICU stay) are shown on the plot on the left. Samples from the consolidated cohorts were partitioned into 8 clusters via k-means clustering, the distribution of which is shown on the tSNE plot on the center. Length of ICU stay is shown on the tSNE plot on the right. Patterns of response for the six interferon response modules across the eight sample clusters are shown on a heatmap below. The red colors indicate that the abundance of transcripts for a given module is predominantly increased with the intensity representing the proportion of constitutive transcripts meeting a given threshold, which at the level of individual samples is a fixed

fold change and difference cutoff ($|\text{Fold change}| > 1.5$, and $|\text{difference}| > 10$ in a given sample over its respective pre-vaccination baseline). The blue color denotes a predominant decrease in abundance of constitutive transcripts compared to the same individual's pre-vaccination baseline. **B.** The heatmap shows patterns of interferon responses for COVID-19 patients with severe disease upon ICU admission. Multiple clinical parameters are shown on the tracks above (ECMO [Extracorporeal Membrane Oxygenation], HTN [Hypertension], CAD [Coronary Artery Disease], CKD [Chronic Kidney Disease], CHF [Congestive Heart Failure]). The histogram represents the length of stay in the hospital, in the ICU, and under mechanical ventilation, in days. **C.** The bar graph represents for different datasets the proportion of samples corresponding to Interferon Response Transcriptional Phenotypes (IRTP) I, II or III, according to the following definition: IRTP I = (S1++S2+", "S1++S20", "S1+S2); IRTP II = (S1++S2++); IRTP III = ("S1-S2++", "S1-S2+", "S10S2++", "S10S2+", "S1-S20"). The datasets in question were derived from the present study: response to COVID-19 mRNA vaccination (N=23) on days 1 and 2 post-prime (P1 and P2, respectively), days 1 and 2 post-boost (B1 and B2, respectively); as well as COVID-19 disease cohorts (PREDICT-19 [N=114] and IMPROVISE [N=]). Others were derived from an earlier study and include reference cohorts of patients with acute influenza infection (FLU, N=25), HIV infection (N=28), active pulmonary tuberculosis (PTB, N=23), acute RSV infection (N=70), bacterial sepsis (N=33) and SLE (N=55).

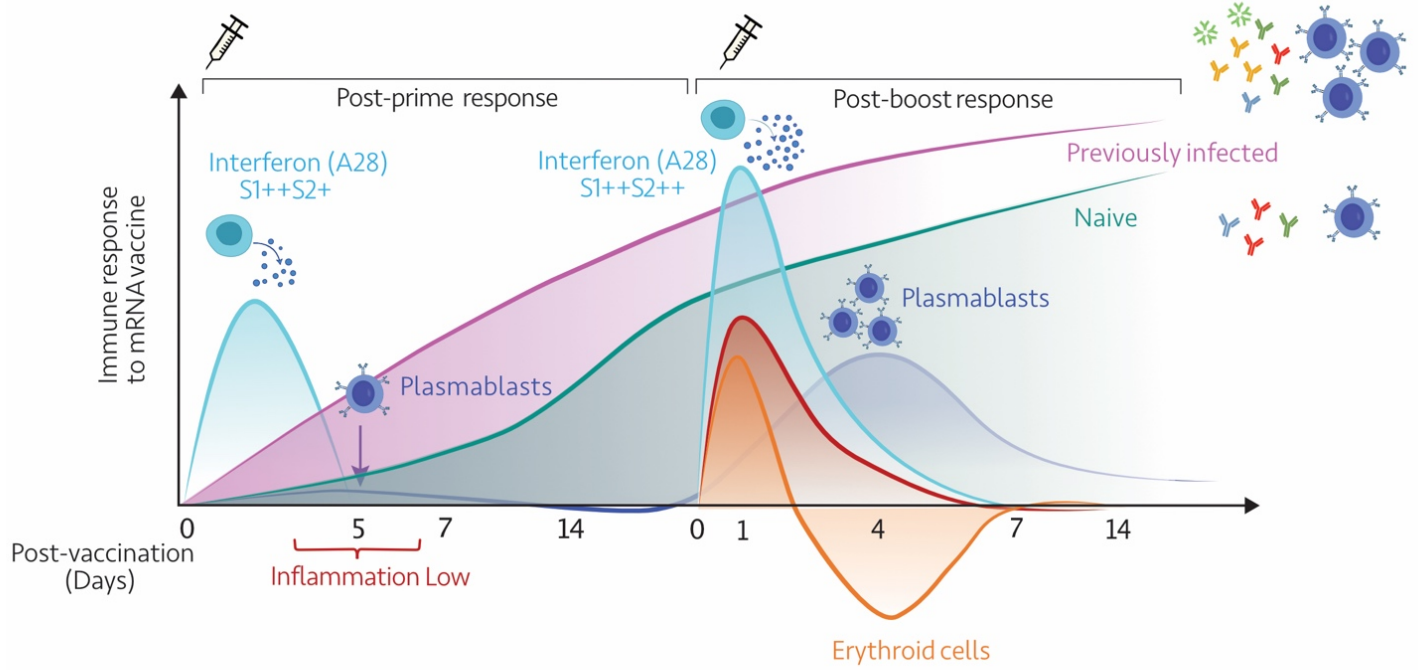


Figure 9: Summary. This diagrammatic representation summarizes the temporal trajectories of blood transcriptional signatures elicited in response to the first and second doses of mRNA vaccines.